Hydrolysis rate constants of ATP up to 120 °C and 1.6 GPa: Implications for life at extreme conditions

Christoph Moeller, Christian Schmidt, Denis Testemale, François Guyot, Maria Kokh, Max Wilke

Hydrolysis rate constants of ATP up to 120 °C and 1.6 GPa: Implications for life at extreme conditions

Christoph Moeller[1*], Christian Schmidt[2], Denis Testemale[3], François Guyot[4], Maria Kokh[1,5], Max Wilke[1]

[1]Institut für Geowissenschaften, Universität Potsdam, Karl-Liebknecht-Straße 24/25, 14476 Potsdam, Germany
[2]Helmholtz-Zentrum Potsdam, Deutsches GeoForschungsZentrum GFZ, Telegrafenberg, 14473 Potsdam, Germany
[3]Néel Institute, Univ. Grenoble Alpes, CNRS 38000 Grenoble, France
[4]IMPMC Muséum National d'Histoire Naturelle, 4 place Jussieu, 75005 Paris, France
[5]Institut für Mineralogie, Universität Münster, Corrensstraße 24, 48149 Münster, Germany

*Corresponding author: chmoeller@uni-potsdam.de

Abstract

Extreme environments are habitats for a diverse array of microorganisms, namely extremophiles, that have evolved unique biochemical adaptations to their geological setting. Some examples of extremophiles can be found in the subseafloor or near hydrothermal vents on the ocean floor. Cultivated strains of extremophiles have demonstrated the ability to tolerate temperatures (T) up to 122 °C and pressures (P) up to 125 MPa. Organisms depend on the stability of key metabolites, such as adenosine triphosphate (ATP), to survive and reproduce under these conditions. In order to maintain their intracellular ATP levels, living cells must compensate for the abiotic hydrolysis of ATP, which occurs at a particularly rapid rate at high temperatures. The role of high pressures and high temperatures in abiotic hydrolysis of ATP has been rarely investigated despite the potential for this phenomenon to contribute to limit the adaptation of microorganisms to simultaneous extreme temperatures and pressures. This study presents new data on the effect of pressure on the abiotic hydrolysis of ATP to adenosine diphosphate (ADP) at elevated temperatures. *In situ* Raman spectra were measured at high pressure and high temperature of the hydrolysis of aqueous disodium ATP solutions in two experimental systems: a hydrothermal diamond anvil cell (HDAC) and a gas-pressurized autoclave. These two systems permitted the determination of hydrolysis rate constants of ATP into ADP up to 1670 MPa at 80 °C, 100 °C, and 120 °C. The data exhibited Arrhenian behavior with a slight decrease in activation energy from 0.5 MPa to 140 MPa. The effect of pressure on ATP hydrolysis rate constants was found to be vanishingly low in the so far known vital range up to 125 MPa. Abiotic hydrolysis rates of ATP showed a pronounced increase at higher pressures. For example, at 100 °C, a rise in pressure from 365 MPa to approximately 1670 MPa results in a nearly tenfold increase in the ATP hydrolysis rate constant. When compared with the typical ATP turnover times reported in living cells, the abiotic ATP hydrolysis rates determined in this study provide insights into the pressure and temperature conditions that could be consistent with living microorganisms.

Keywords: Raman spectroscopy, adenosine triphosphate (ATP), adenosine diphosphate (ADP), hydrothermal diamond anvil cell (HDAC), autoclave, sapphire cell, high pressure, high temperature

1. Introduction

The study of extremophiles, microorganisms that thrive under extreme temperature (T) and pressure (P) conditions (Macelroy, 1974), has broadened our understanding of the potential for life beyond previously known boundaries. In the 1970s, the discovery of biological communities living near hydrothermal vents on the ocean floor, an environment that seemed inhospitable, came as a surprise and challenged conventional perspectives of habitability (Corliss and Ballard, 1977). In these conditions, organisms are capable of growth and reproduction at temperatures up to 110 °C to 120 °C and at hydrostatic pressures ranging from 20 MPa to 40 MPa (Delaney et al., 1992; Glickson et al., 2007; Blöchl et al., 1997; Edwards et al., 2011). More recent findings in the deep subseafloor have demonstrated significant microbial activity up to 120 °C (Heuer et al., 2020). Currently, two cultivated strains of hyperthermophilic archaea isolated from ocean floor hydrothermal vents tentatively set the known P-T limits for life. *Methanopyrus kandleri sp.* exhibits cell growth up to 122 °C at 20 MPa (Takai et al., 2008), while *Thermococcus piezophilus sp.* is capable of surviving up to 125 MPa at 65 °C to 95 °C (Dalmasso et al., 2016). Raman spectroscopic investigations of *Shewanella oneidensis sp.* in a diamond anvil cell have suggested the possibility of life at pressures up to the gigapascal range (Sharma et al., 2002). However, the criterion for a viable state, namely formate oxidation, has been heavily criticized and is indeed very ambiguous (e.g., Yayanos, 2002).

In directed evolution studies, the mesophilic bacterium *Escherichia coli sp.* demonstrated the ability to develop resistance to high pressure within a short period of time (Vanlint et al., 2011). Traditional cultivation experiments on piezophiles from the deep biosphere are extremely challenging due to their incredibly slow growth rates with a cell division down to once per 1000 years (e.g., Jørgensen, 2011). Therefore, it would not come to a surprise that organisms may live beyond currently defined pressure boundaries. In order to live under these conditions, organisms would have to maintain an active metabolism. Consequently, a study of the physicochemical properties of key metabolites is essential to comprehend potential survival strategies of life. Up to 2000 MPa, pressure can alter intermolecular distances and conformational states of molecules in cells, whereas the covalent bond distances and bond angles of a molecule remain unchanged (Jebbar and Oger, 2010). These changes can result in alterations to kinetic parameters, thermodynamic equilibrium constants, folding profiles and ligand bindings of proteins and organic compounds (Bridgman, 1914; Kauzmann, 1987; Urayama et al., 2002). Among essential metabolites are adenosine triphosphate (ATP), adenosine diphosphate (ADP), and adenosine monophosphate (AMP).

In living cells, enzymes catalyze the endergonic phosphorylation of ADP to ATP through various pathways including oxidative phosphorylation catalyzed by membrane-bound ATP synthase or substrate-level phosphorylation. The exergonic hydrolysis of ATP is then coupled with other vital endergonic biochemical reactions. In other words, ATP carries chemical energy by transferring a phosphoryl group from a donor to an acceptor (Burgot, 2019). This mechanism is universal in all metabolic systems; thus, ATP was coined the universal biological energy currency (Lipmann, 1941). To ensure their vital functioning, living cells use redox reactions to maintain a steady state of ATP to ADP ratios far from thermodynamic equilibrium. Rapid abiotic ATP hydrolysis kinetics thus implies higher maintenance energy costs for cells, and it has

been suggested that this is an important factor in setting the limits to the functioning of living organisms (Bains et al., 2015).

A number of studies have been conducted to ascertain the kinetic effects of temperature and chemical environment on ATP hydrolysis. The increase in hydrolysis rate with temperature is well described by an Arrhenius relation (Hulett, 1970; Leibrock et al., 1995; Daniel et al., 2004; Moeller et al., 2022). The addition of metal cations can result in a deceleration of the hydrolysis rate as observed for Ca or Mg (Ramirez et al., 1980; Leibrock et al., 1995), or an acceleration as demonstrated for Cu (II) (Buisson and Sigel, 1974) or Co (III) complexes (Suzuki et al., 1978). Moeller et al. (2022) estimated a temperature of about 200 °C at which abiotic ATP hydrolysis would not be compensated by normal cellular regeneration time. This suggests that the abiotic hydrolysis of ATP is unlikely to be the main factor determining the upper temperatures recorded for microbial life. Nevertheless, the question of the cross-effect of pressure on this temperature limit remains unanswered, despite its importance, given that the subsurface or ocean floor deep biospheres are indeed subjected to high pressures. The effect of pressure on abiotic ATP hydrolysis has so far been studied only by Leibrock et al. (1995). The authors observed that the hydrolysis of ATP-D_2O at 80 °C was accelerated from 10 MPa to 120 MPa and then decelerated from 120 MPa to 220 MPa.

Moeller et al. (2022) introduced a protocol to directly study ATP hydrolysis at high temperature using *in situ* Raman spectroscopy. *In situ* Raman spectroscopy is an efficient technique utilized across scientific disciplines, including high pressure biology, to monitor the effects of different pressures, temperatures, and chemical environments on the kinetics of biochemical reactions. In the present study, Raman spectroscopy combined with a hydrothermal diamond anvil cell (HDAC) was employed to obtain *in situ* measurements of abiotic ATP hydrolysis under pressures up to 2000 MPa. To improve the pressure resolution, particularly below 140 MPa, an *in situ* Raman setup based on an autoclave fitted with optical high-pressure windows was utilized.

2. Materials and methods

2.1. Sample preparation

Ultrapure adenosine triphosphate disodium salt $C_{10}H_{14}N_5Na_2O_{13}P_3Na_2 \cdot 3\ H_2O$ with a purity of 98%, hereafter referred to as ATP, was purchased from VWR (VWR, Germany). This compound was chosen to be comparable to previous data (e.g., Leibrock et al., 1995; Moeller et al., 2022). In the hydrothermal diamond anvil cell, Milli-Q water purification system water was used for experiments, while high-performance liquid chromatography (HPLC) water was used in the autoclave due to availability. Pure deuterated water (D_2O) was also utilized as a solvent. Solutions were prepared by weighing and dissolving 0.1 mol/l ATP in water by manually stirring and gently shaking the sample container. This concentration of Na_2H_2ATP corresponds to the solubility product. A notable increase in concentration due to evaporation would result in the precipitation of Na_2H_2ATP, which was not observed. The error of weighing was less than 0.003 g. Each solution was prepared with a minimum volume of 3 ml. The resulting concentration of ATP was 0.1 mol/l ± 0.009 mol/l. All solutions were transparent without visible precipitates. The initial pH was measured with Endress and Hauser electrodes at room temperature and repeatedly controlled with indicator paper. The pH of the ATP-H_2O solutions varied from 2.8 to 3.0, while the pD of ATP-D_2O solutions was 3.3 to 3.5. This difference is within

the error of the general pD/pH relationship of pD = pH + 0.41 (Covington et al., 1968). Note that the pH was not buffered during the experiments.

2.2. Isobaric experiments using an autoclave

For isobaric experiments, samples were loaded into a sapphire reaction cell, which was installed within a high-pressure autoclave (Testemale et al., 2005; Louvel et al., 2015). The autoclave was pressurized by helium (He) and was fitted with high-pressure optical windows made of sapphire. A double wall system of the autoclave enabled cooling by water. The sapphire cell was 100 mm in length and had an inner diameter of 5 mm. It was manufactured by R.S.A. le Rubis SA, France. The sample was contained within the tube between two moving pistons of vitreous carbon, which transmitted the pressure of the helium to the solution. Two silicone O-rings were used to seal the cell, between pistons and tube. The sample volume was about 0.2 ml.

Pressure and temperature were controlled independently by Eurotherm® controllers. The pressure regulation had a precision of ±0.2 MPa (Bruyere et al., 2008). Heating was provided by a resistive furnace made of 0.4 mm diameter molybdenum (Mo) wire wrapped around a cylindrical Mo heat distributor in which the sample cell was placed. K-type thermocouples were placed inside the distributor. The temperature was measured with a precision of ±0.1 °C. The discrepancy between the thermocouples and the sample was 10 °C. The overall uncertainty on temperature was estimated to be ±5 °C. The target temperature and pressure were reached within two to three minutes.

The apparatus was attached to a Princeton SpectraPro SP2758 Raman spectrometer. A diode-pumped solid-state laser (Cobolt Fandango 100) of 515 nm was used for excitation. The laser power was 80 mW without objective before the laser beam entered the autoclave. A diffraction grating of 1800 lines/mm and edge filters were installed. Only the 1800 lines/mm grating had a sufficient resolution of 1 cm^{-1} for the peak-fitting-model applied later. A CCD Pylon detector with 1340 pixels measured the Raman scattering. It was cooled with liquid nitrogen at -120 °C. Spectra were acquired every 30 seconds as an average of three accumulations of nine seconds each. Each data set was acquired sequentially under isothermal and isobaric conditions. The temperatures of the experiments were 80 °C, 100 °C and 120 °C. The pressure of the experiments ranged from 0.5 MPa to 140 MPa. Figure 1 illustrates exemplary timeseries of each ATP solution and sample holder.

2.3. Experiments using a hydrothermal diamond anvil cell

A Bassett-type hydrothermal diamond anvil cell, HDAC (Bassett et al. 1993; Schmidt and Chou, 2021), was utilized for experiments ranging from vapor-saturated pressure (Psat) to 2000 MPa at 80 °C, 100 °C and 120 °C. The cell was equipped with colorless ultra-low fluorescence and ultra-low birefringence diamond anvils with a diameter of the culet faces of 0.9 mm. The solution was loaded into the sample chamber, which was formed by a cylindrical hole in an iridium (Ir) gasket. The initial diameter of the sample chamber was 300 µm with a height of 125 µm. A quartz grain was added into the cell as a Raman spectroscopic pressure sensor. The pressure was determined by measuring the shift of the Raman band at 465 cm^{-1} (Schmidt and Ziemann, 2000). The position of the mercury (Hg) line at 546 nm from a fluorescent lamp was simultaneously monitored to correct the Raman band position if required. The Raman spectrum of the quartz grain was recorded before the experiment at room temperature and after the

experiment at target temperature to minimize delays in measuring the reaction kinetics. The Ir gasket may shrink upon heating leading to a slight volume change. This change is known to occur rapidly after reaching the temperature with no further change over run time (Schmidt and Ziemann, 2000). Gasket failure due to expansion resulting in a larger sample chamber diameter or deviations from a circular shape has not been observed. The temperature effect on the peak position was corrected using the equation provided by Schmidt and Ziemann (2000).

The pressure accuracy is approximately ±30 MPa (Schmidt, 2009). The temperature was measured by two K-type thermocouples attached to the anvils. The power input to two resistive heaters, Ni-Cr coils around the seats, was controlled using Eurotherm® temperature controllers. The target temperature was reached within one minute. The overall uncertainty in the temperature was ±1 °C.

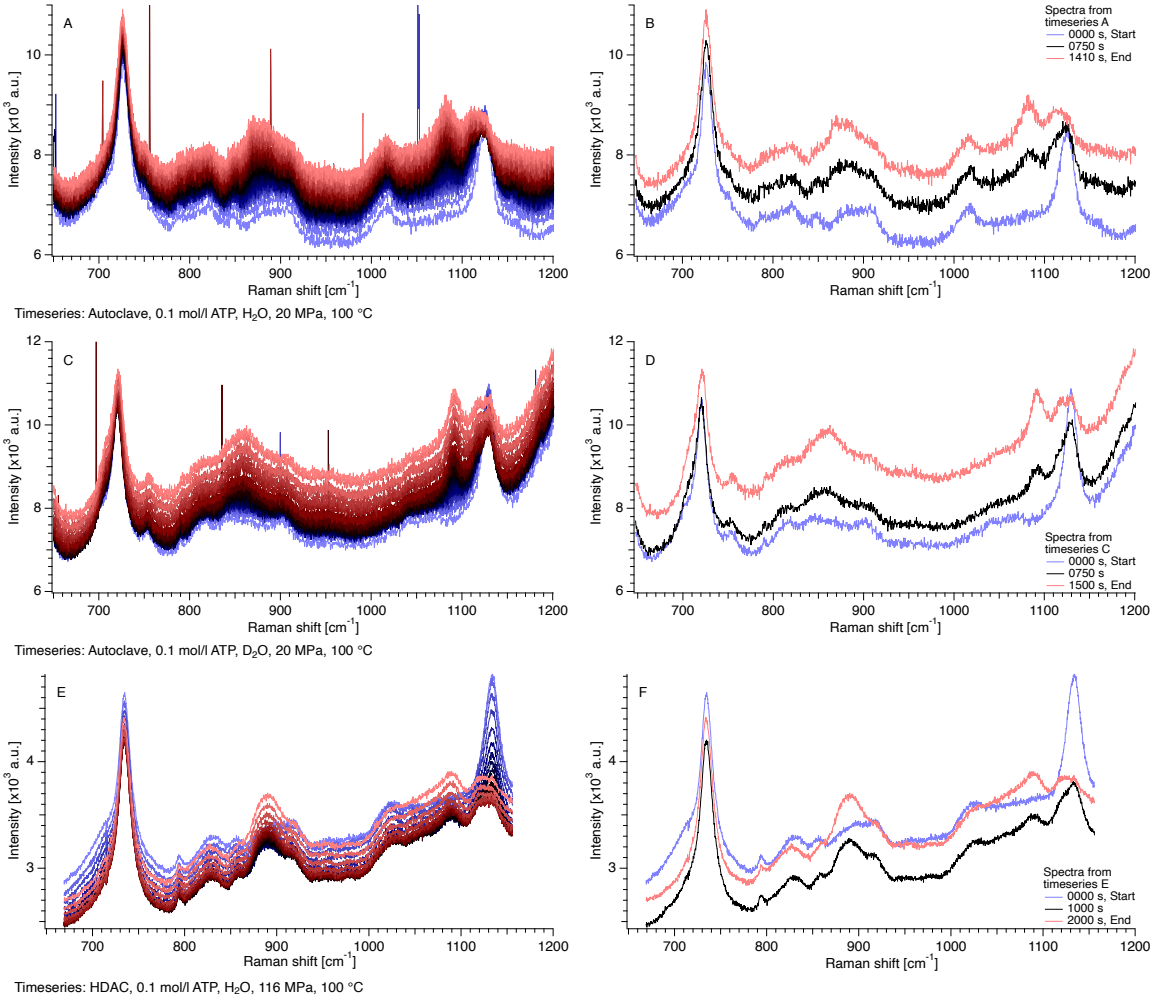

Figure 1: Exemplary Raman spectra as a function of time (on the left) and Raman spectra showing the first, an intermediate and the final Raman spectrum of the timeseries (on the right). A and B: Timeseries of 0.1 mol/l ATP-H_2O obtained in the autoclave at 100 °C and 20 MPa. C and D: Timeseries of 0.1 mol/l ATP-D_2O obtained in the autoclave at 100 °C and 20 MPa. E and F: Timeseries of 0.1 mol/l ATP-H_2O obtained in the HDAC at 100 °C and 116 MPa.

The Raman spectrometer was a HORIBA Jobin Yvon LabRAM HR800 VIS equipped with an Olympus BXFM confocal microscope and a motorized XYZ stage. A frequency-doubled Nd:YAG laser with a wavelength of 532 nm was used for excitation. The laser power was 32 mW without objective before the laser beam entered the HDAC. The objective was an Olympus SLMPlanN 20× with a working distance of 25 mm. A diffraction grating with 1800 lines/mm,

a Peltier-cooled CCD detector with 1024 x 256-pixels, and edge filters were installed. The Raman spectra were acquired as an average of five accumulations of 20 seconds each.

2.4. Experimental data treatment

The recorded ranges of the Raman spectra were 647 cm^{-1} to 1200 cm^{-1} in the autoclave and 669 cm^{-1} to 1155 cm^{-1} in the HDAC. The intensity of the Raman scattering in the autoclave was approximately two to three times higher than that collected in the HDAC. An increasing luminescence effect was visible in the spectra when AMP formed in the solution. All raw spectra are available in the Data Availability section ([dataset] Moeller et al., 2024).

The symmetric stretching mode ν_s of the terminal phosphate group PO_2 (OH) at 1080 cm^{-1} for AMP, at 1110 cm^{-1} for ADP, and at 1120 cm^{-1} for ATP was used to detect the relative change in the respective species concentration. The ring vibration at 728 cm^{-1} of the adenosine moiety ν_{ring} (C–C, N–C) was exclusively assigned to the adenosine moiety (Mathlouthi et al., 1984; Rimai et al., 1969). Therefore, it could be used as an internal standard for Raman intensity (Moeller et al., 2022). Comparative measurements on solutions of 0.1 mol/l ATP and ADP demonstrate that the ring vibration is identical within the usual measurement inaccuracies (Figure 2).

The spectra of the solutions were divided into two sections to allow a linear baseline subtraction. This was done by dividing the spectra into two sections, one ranging from 666 cm^{-1} to 785 cm^{-1} and the other from 978 cm^{-1} to 1155 cm^{-1} for spectra obtained using the HDAC (Figure 3, A-B). Similarly, the spectra were divided into two sections, one ranging from 662 cm^{-1} to 778 cm^{-1} and the other from 965 cm^{-1} to 1198 cm^{-1} for spectra acquired using the autoclave in the presence of water (Figure 3, C-D). For spectra obtained in the autoclave in the presence of deuterated water (Figure 3, E-F), the ranges were 662 cm^{-1} to 778 cm^{-1} and 1067 cm^{-1} to 1152 cm^{-1}. The addition of peaks to the peak-fitting model ensured the stability and consistency of the procedure throughout the entire series. The peak assignments are provided in Table 1, along with the initial peak positions of the peak-fitting model. It is notable the position of the Raman band of the terminal phosphate group PO_2 (OH) at 1080 cm^{-1} (AMP), at 1110 cm^{-1} (ADP) and at 1120 cm^{-1} (ATP) at ambient conditions shifts considerably with pressure. To compensate for this effect in the high-pressure (HP) experiments in the HDAC, and to ensure a robust fit, the initial peak positions of these modes were shifted. The maximum shift was 10 cm^{-1} for the adenosine polyphosphate bands in H_2O solutions.

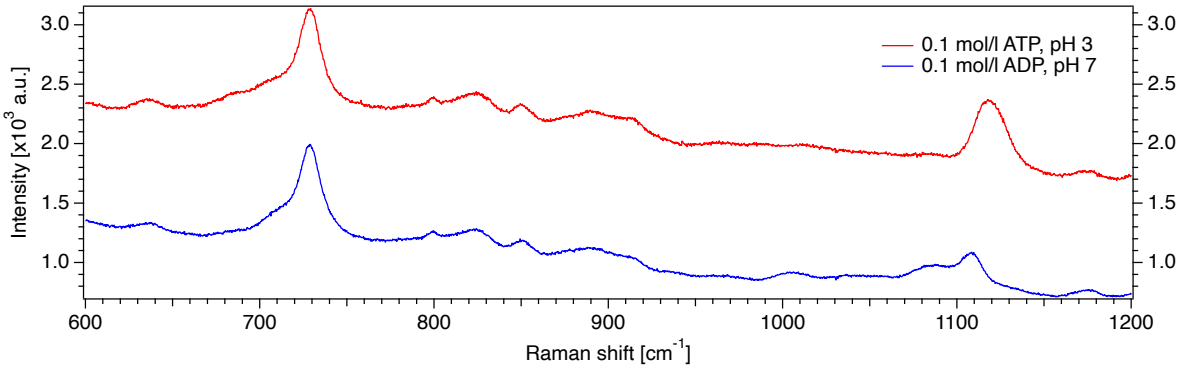

Figure 2: Raman spectra of 0.1 mol/l ATP and ADP solutions measured in a quartz cuvette at ambient conditions.

Table 1: Assignment of the vibrational modes of the measured Raman spectra to literature values for the spectra of ATP-H_2O/D_2O solutions in the HDAC and the autoclave (n.a. = not assigned).

Peak position [cm^{-1}] – peak-fitting-model					
Reference	**H_2O^H**	**H_2O^S**	**D_2O^S**		**Reference**
713	720	700	720	ν_s (POP)	Eysel and Lim (1988)
727-731	729	727^L	729^L	ν_{ring} (C-C, N-C)	Mathlouthi et al. (1984), Rimai et al. (1969)
755		752	755	Sapphire signal	n.a.
984	990			ν_{as} POP (Fermi level)	Eysel and Lim (1988), Marshall and Begun (1989)
1008	1010	1015		ν_{as} $P(OH)_3$	Rudolph (2010)
1045	1045	1035		n.a.	n.a.
1065	1065	1060		n.a.	n.a.
1080	1080	1083	1090	ν_s PO_2 (OH), AMP	Rimai et al. (1969)
1097	1096	1096		ν_e PO_3	Eysel and Lim (1988)
1110	1111	1111	1110	ν_s PO_2 (OH), ADP	Rimai et al. (1969)
1120	1123-1130	1124-1130	1125^L	ν_s PO_2 (OH), ATP	Rimai et al. (1969), Heyde and Rimai (1971)
1128	1140		1130	ν_e PO_3	Eysel and Lim (1988), Preston and Adams (1979)
1150		1160		ν_{as} PO_2	Eysel and Lim (1988), Marshall and Begun (1989)

^{H}HDAC; ^{S}Sapphire cell; ^{L}Lorentzian distribution

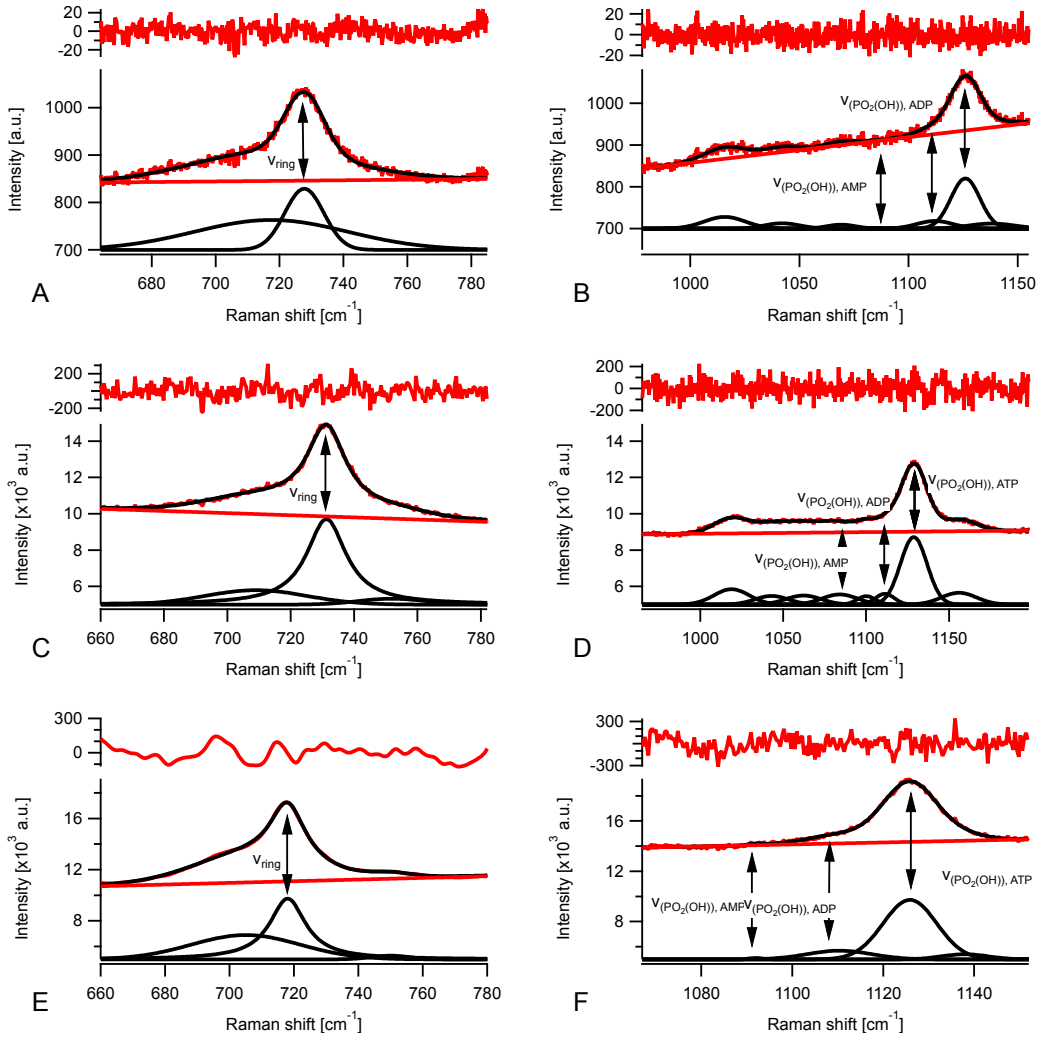

Figure 3: Peak-fitting-model after Moeller et al. (2022), were applied to the measured timeseries. The main peaks are marked and further described in the text. A) ATP + H_2O obtained in a HDAC in the range from 660 v to 785 cm^{-1}. B) ATP + H_2O obtained in a HDAC in the range from 978 cm^{-1} to 1155 cm^{-1}. C) ATP + H_2O obtained in the autoclave in the range from 660 $cm^{-1}$to 785 cm^{-1}. D) ATP + H_2O obtained in the autoclave in the range from 965 cm^{-1} to 1198 cm^{-1}. E) ATP + D_2O obtained in the autoclave in the range from 662 cm^{-1} to 778 cm^{-1}. F) ATP + D_2O obtained in the autoclave in the range from 1067 cm^{-1} to 1152 cm^{-1}.

The symmetric stretching mode ν_s of the terminal phosphate group PO_2 (OH) of ADP at 1110 cm^{-1} and ATP at 1120 cm^{-1} are partly overlapping (Figure 2) which resulted in less accurate results in unconstraint fits. To achieve maximum flexibility and to maintain the fit approach stable throughout the reaction, a minimum of fitting constraints was chosen. The peak position was allowed to vary within 3 cm^{-1} to 5 cm^{-1}. To prevent the occurrence of large, flat peaks, the width of ν_s (PO_2 (OH)) of ATP from the very first spectra in the timeseries was employed as a constraint for the peak width of all peaks. Peak height and width were constrained to be positive.

The integrated intensity of the ν_s (PO_2 (OH)) peak was normalized to that of ν_{ring} (C–C, N–C). Both values were corrected for temperature (Brooker et al., 1988) and excitation efficiency (Schmidt et al., 2009). The result was a measure of the concentration of [ATP] without further calibration as only the relative changes are of interest for the determination of the rate constant. Rate constants for the reaction of ATP to ADP were calculated assuming a first order reaction (Khan and Mohan, 1974). The formation of diphosphate from the reaction of ATP to AMP has not been reported in experimental studies (Leibrock et al., 1995). Therefore, the concentration of the reactant as a function of time t can be described by

$$ln\left(\frac{[ATP]_t}{[ATP]_0}\right) = -kt \qquad \text{Eq. 1}$$

and the corresponding half-life $t_{1/2}$ can be determined by

$$t_{1/2} = \frac{\ln 2}{k} \qquad \text{Eq. 2}$$

where $[ATP]_t$ is the concentration of ATP at time t, $[ATP]_0$ the concentration at t = 0, and the rate constant k. The constant can be determined by substituting the reduced intensity for the concentration in Eq. 1. The slope of a linear fit is the rate constant k. By convention, k is positive. During the fit the y-intercept was set to 0. Representative fits for datasets from the autoclave are shown in Figure 4. The lowest values of $\ln([ATP]_{i,t}/[ATP]_{i,0})$ included in the fits were -1 for data in the autoclave and -1.6 for data in the HDAC. All fitted lines consisted of at least three points, except for one data set at 120 °C and 176 MPa in the HDAC due to the insufficient temporal resolution of 100 s/spectrum of the HDAC; therefore, it has a presumably much higher uncertainty. The qualitative detection limits of the setups are around 0.005 mol/l, which is equivalent to 5% of the initial ATP concentration. The limit of the peak-fit-model was approximately 0.025 mol/l, which is 25% of the initial ATP concentration. Exemplary peak-fitting-models, the assignment of the peaks, and all intermediate results are available in the Data Availability section ([dataset] Moeller et al., 2024).

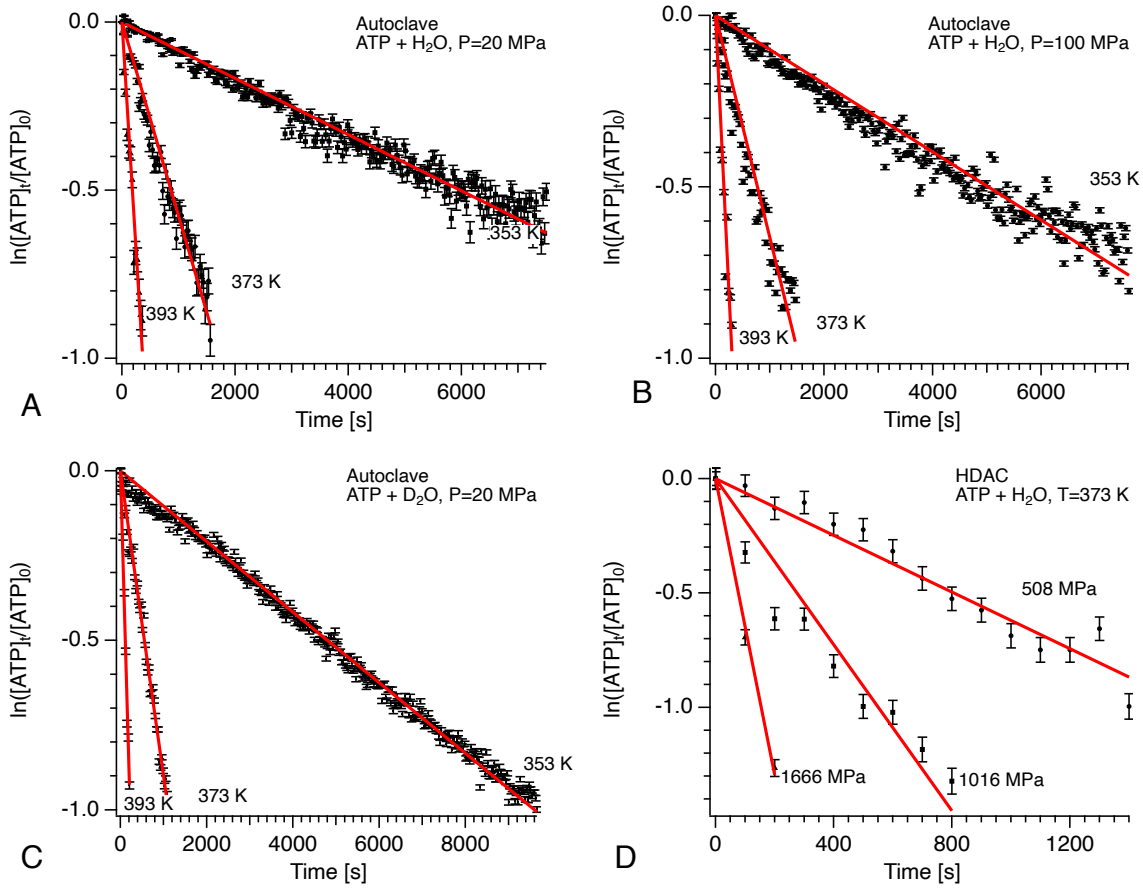

Figure 4: Linear fits of ln([ATP]t/[ATP]$_0$) vs Time, where the slope is k. Datasets A-C were determined in the autoclave. Dataset D was obtained from the HDAC. A) Linear fits of datasets at 20 MPa and H_2O. B) Linear fits of datasets at 100 MPa. C) Linear fits of datasets of ATP-D_2O solutions at 20 MPa. D) The linear fits of the datasets obtained at high pressure in the HDAC at 100 °C are presented below.

2.5. Thermodynamic calculations of pH during ATP hydrolysis

For the thermodynamic properties of ATP, a distinction is made between Mg-Ca and Mg-Ca-free systems, as Mg^{2+} and Ca^{2+} are known to form complexes with ATP (Alberty, 1969; Gajewski et al., 1986; Phillips et al., 1966). In the present study, it is assumed that Na^+ ions do not form complexes with ATP and its hydrolysis components. The system components chosen for the thermodynamic modeling are listed in Table 2 and include water, dissolved organic and inorganic aqueous species, and real gases. The provided data are only applicable for the P-T conditions of our experiments. The Haar-Gallagher-Kell and Marshall and Franck models (Marshall and Franck, 1981; Kestin et al., 1984) were employed to determine the thermodynamic properties and dissociation constant of H_2O for the experimental conditions. The Helgeson-Kirkham-Flowers (HKF) equation of state (Helgeson et al., 1981) was employed for aqueous species, while the Peng-Robinson equation of state (Peng and Robinson, 1978) was utilized for aqueous vapor and solid phases. The HKF equation of state is applicable up to 500 MPa.

Table 2: The system components chosen for the thermodynamic modeling and the corresponding thermodynamic data sources.

Species	Charge	Chemical Formula of organic aqueous species	Reference
Solid phase			
Quartz (SiO_2)	0		Robie and Hemingway (1978)
Aqueous solution			
H_2O	0		Marshall and Franck 1981; Kestin et al. (1984)
OH^-	1-		Shock et al. (1997),
H^+	1+		zero by definition
PO_4^{3-}	3-		Shock and Helgeson (1988)
HPO^{4-}	4-		Shock et al. (1997)
$H_2PO_4^{2-}$	2-		Shock et al. (1997)
H_3PO_4 (aq)	0		Shock et al. (1989)
Na^+	1+		Shock et al. (1997)
NaOH (aq)	0		Shock et al. (1997)
SiO_2 (aq)	0		Sverjensky et al. (2014)
Si_2O_4 (aq)	0		Sverjensky et al. (2014)
N_2 (aq), O_2 (aq), H_2 (aq)	0		Robie and Hemingway (1978)
AMP^{2-}	2-	$C_{10}H_{12}N_5O_7P$	LaRowe and Helgeson (2006)
$HAMP^{1-}$	1-	$C_{10}H_{13}N_5O_7P$	LaRowe and Helgeson (2006)
H_2AMP (aq)	0	$C_{10}H_{14}N_5O_7P$	LaRowe and Helgeson (2006)
ADP^{3-}	3-	$C_{10}H_{12}N_5O_{10}P_2$	LaRowe and Helgeson (2006)
$HADP^{2-}$	2-	$C_{10}H_{13}N_5O_{10}P_2$	LaRowe and Helgeson (2006)
H_2ADP^{1-}	1-	$C_{10}H_{14}N_5O_{10}P_2$	LaRowe and Helgeson (2006)
H_3ADP (aq)	0	$C_{10}H_{15}N_5O_{10}P_2$	LaRowe and Helgeson (2006)
ATP^{4-}	4-	$C_{10}H_{12}N_5O_{13}P_3$	LaRowe and Helgeson (2006)
$HATP^{3-}$	3-	$C_{10}H_{13}N_5O_{13}P_3$	LaRowe and Helgeson (2006)
H_2ATP^{2-}	2-	$C_{10}H_{14}N_5O_{13}P_3$	LaRowe and Helgeson (2006)
H_3ATP^{1-}	1-	$C_{10}H_{15}N_5O_{13}P_3$	LaRowe and Helgeson (2006)
H_4ATP (aq)	0	$C_{10}H_{16}N_5O_{13}P_3$	LaRowe and Helgeson (2006)
Gaseous mixture			
H_2O (g)	0		Robie and Hemingway (1978)
N_2 (g)	0		Robie and Hemingway (1978)

The HCh software (Shvarov, 1999) was used to calculate the pH of the experimental solutions under study at specified P-T conditions. HCh minimizes the total Gibbs free energy of the system, thereby providing the concentrations of the system components, their activity coefficients, the ionic strength of an aqueous solution, and its pH and Eh. In order to model the pH at elevated temperatures, pH_T, in our experiments, it was assumed that 0.1 mol of Na_2H_2ATP dissociates completely in 1 kg of H_2O, forming H_2ATP^{2-} and 2 Na^+. The reactions involved in the hydrolysis of ATP to ADP can be summarized by the following equation (Eq. 3):

$$H_xATP^{x-4} + H_2O \rightarrow H_yADP^{y-3} + HPO_4^{2-} + H^+ \qquad \text{Eq. 3}$$

with values of x between 0 and 4 and values of y between 0 and 3. To simulate the effect of the additional phases in our system, the partition of H_2O from the liquid phase to the vapor phase at Psat was calculated. The effect of quartz dissolution at equilibrium conditions was simulated by the addition of one mole of quartz to the solution. To calculate the metastable equilibrium conditions, where the ATP hydrolysis progresses step-by-step, the following steps were calculated: first, forming ATP species in a calculated system with one liquid phase containing ATP species (l_1), and then, dissociating further to form ADP and AMP species in calculated systems with one liquid phase containing ATP and ADP species (l_2) and one liquid phase containing ATP, ADP and AMP species (l_3,), respectively. These system compositions served as the basis for the thermodynamic simulations. To simulate a potential exchange reaction of H_2O from the liquid to the vapor phase, a nitrogen phase was added to the system and gaseous H_2O (g) was

allowed to fractionate to the vapor phase which is designated as "+v". To simulate the role of quartz in the system, quartz was included in the thermodynamic model which is designated as "+q".

The pH was calculated in 12 distinct model systems, including single aqueous solutions (l_1, l_2, l_3), two-phase systems with an aqueous solution and a vapor phase (l_1+v, l_2+v, l_3+v, l_1+v_c, l_2+v_c, l_3+v_c) and two-phase systems with an aqueous solution and a quartz grain (l_1+q, l_2+q, l_3+q) (Table 3). Thus, it was possible to simulate the pH at equilibrium conditions in three types of experimental systems: a single-phase isothermal-isobaric aqueous system applicable to our experiments in the autoclave, a single-phase isothermal-isochoric aqueous system with a quartz grain as a pressure sensor applicable to our experiments in the HDAC and a two-phase aqueous system applicable in the HDAC that were performed at Psat.

Table 3: Initial chemical phase composition of the thermodynamic calculations.

System name	System components
l_1	H_2O, H^+, OH^-, Na^+, NaOH (aq), O_2 (aq), H_2 (aq), N_2 (aq), PO_4^{3-} HPO_4^{2-}, $H_2PO_4^-$, H_3PO_4 (aq), ATP^{4-}, $HATP^{3-}$, H_2ATP^{2-}, H_3ATP^{1-}, H_4ATP (aq)
l_2	aqueous fluid of system l_1+ ADP^{3-}, $HADP^{2-}$, H_2ADP^-, H_3ADP (aq)
l_3	aqueous fluid of system l_2+ AMP^{2-}, $HAMP^{1-}$, H_2AMP (aq)
l_1 + v	aqueous fluid of system l_1 + N_2 (g), H_2O (g)
l_2 + v	aqueous fluid of system l_2 + N_2 (g), H_2O (g)
l_3 + v	aqueous fluid of system l_3 + N_2 (g), H_2O (g)
l_1 + q	aqueous fluid of system l_1 + SiO_2 (aq), Si_2O_4 (aq), quartz
l_2 + q	aqueous fluid of system l_2 + SiO_2 (aq), Si_2O_4 (aq), quartz
l_3 + q	aqueous fluid of system l_3 + SiO_2 (aq), Si_2O_4 (aq), quartz

3. Results

Table 4 and Figure 5 summarizes all 49 hydrolysis rate constants and their respective half-lives. These include 40 for the ATP-H_2O system and 9 for the ATP-D_2O system. Of these, 38 were determined in the autoclave, while 11 were measured in the HDAC. In addition to the experimental kinetic data, thermodynamically calculated pH values at these P-T conditions are provided at run conditions (Table 4). It should be noted that the calculation of ion concentrations and thus a pH above 500 MPa is limited by the HKF equation of state. Figure 5 depicts the distribution of these rate constants as a function of pressure. A standard deviation (σ_1) for the rate constant was determined by performing three experiments at 20 MPa in the autoclave, each at temperatures of 80 °C, 100 °C, and 120 °C. The standard deviations ranged from 4% to 9.5% relative to the value of the rate constant. To be conservative, a standard deviation of 10% was assumed for data sets in the autoclave. It is not possible to reproduce single fluid aqueous experiments in the isochoric HDAC at the exact same conditions due to technical limitations. Nevertheless, a replication of the experiment at Psat of Moeller et al. (2022) demonstrated a standard deviation of 5.5%, which is within the estimated standard deviation of 10%. It can therefore be reasonably assumed that the overall precision of both apparatuses and the fitting procedure is 10%. The data encompass a pressure range from Psat to 1670 MPa and temperatures of 80 °C, 100 °C, and 120 °C (Table 4). Additionally, datasets from Leibrock et al. (1995) and Moeller et al. (2022) are provided for comparison.

The results are in satisfactory agreement with previous studies in the overlapping pressure and temperature domains as illustrated in Figure 5. There is also satisfactory agreement between the hydrolysis constants measured in the autoclave and in HDAC when pressures and temperatures overlap. Finally, ATP hydrolysis rates exhibited a significant increase with pressure

when the latter exceeds 800 MPa. Each temperature series of the constants obtained in the autoclave for the hydrolysis in H_2O follows a similar trend with pressure. The ATP hydrolysis rate exhibits an average increase of 1.14 ± 0.11 at 80 °C, 1.32 ± 0.05 at 100 °C and 1.14 ± 0.07 at 120 °C between 0.5 and 20 MPa. The rate constants fluctuate around an average value which is 10.7×10^{-5} s^{-1} ± 2.5×10^{-5} s^{-1} at 80 °C, 7.5×10^{-4} s^{-1} ± 1.6×10^{-4} s^{-} at 100 °C and 3.8×10^{-3} s^{-1} ± 0.85×10^{-4} s^{-1} 120 °C for the pressure range of 20 MPa to 100 MPa. The rate constants show a slight increase from 100 MPa to 140 MPa with a factor of 1.32 ± 0.02. The overall increase from 0.5 MPa to 140 MPa is by a maximum factor of 1.7 ± 0.08. In the autoclave, the lowest achievable pressure for all three temperatures was 0.5 MPa. The data are generally consistent with the Psat data of Moeller et al. (2022), although some minor systematic differences can be observed. Autoclave values appear to be larger by a factor of approximately 1.3 at 80 °C, identical within the σ_1 of 10% at 100 °C, and smaller by a factor of approximately 0.7 at 120 °C. The hydrolysis rate constants obtained in the HDAC in the overlapping pressure range plot slightly below the autoclave data. The HDAC at 80 °C and 90 MPa and at 120 °C and 176 MPa data are lower than the autoclave data at 80 °C and 120 °C and at 100 MPa by a factor of 1.13 ± 0.01. At 100 °C, the ratio of the HDAC data at 116 MPa to the autoclave data at 100 MPa is approximately 1.6. However, at 80 °C, both datasets demonstrate a moderate increase in the rate constants within the pressure ranges of 0.1-90 MPa for the HDAC and 0.5-100 MPa for the autoclave, with a moderate increase of the rate constants by a factor of 1.34 ± 0.07.

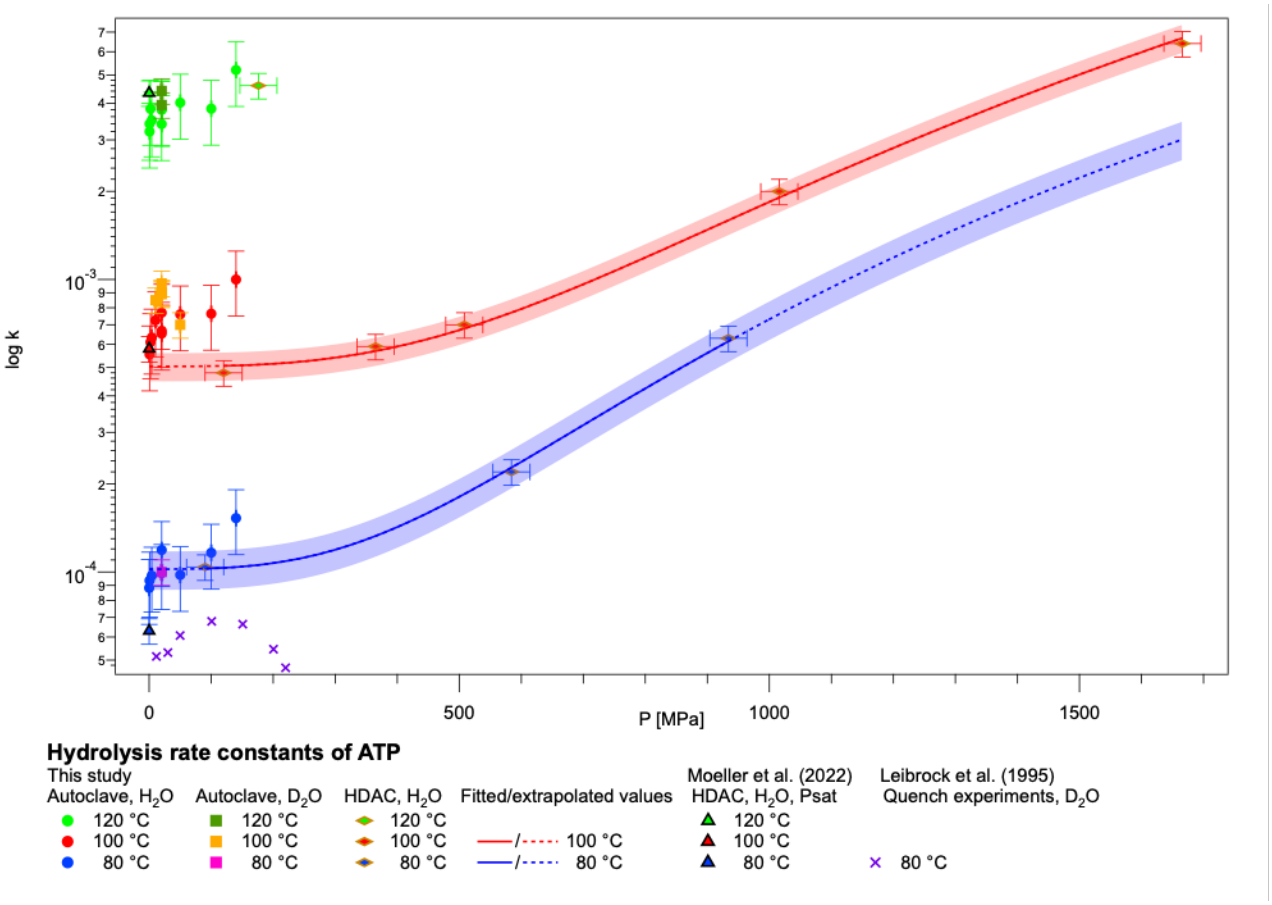

Figure 5: Hydrolysis rate constants of ATP in H_2O/D_2O taken in the course of this study. It is shown the range of 0-1700 MPa. The data from Moeller et al. (2022) and Leibrock et al. (1995) are plotted for comparison.

347 *Table 4: Hydrolysis rate constants of ATP for solutions with H_2O and D_2O with corresponding half-lives determined in the*
348 *HDAC and autoclave. A pH at run conditions was thermodynamically calculated based on the phase composition l_1, l_2, l_3,*
349 *l_1+q, l_2+q, l_3+q, l_1+v, l_2+v, l_3+v described in Table 3. The calculation of pH values above 500 MPa is limited by the HKF*
350 *equation of state.*

Hydrolysis rate constants obtained in the autoclave				**Calculated pH**		
T [°C] ± 1 [°C]	**P [MPa] ± 0.2 [MPa]**	**k [× 10^{-3} s^{-1}] ± 10%**	**$t_{1/2}$ [s] ± 10%**	**l_1**	**l_2**	**l_3**
80	0.1	9.09×10^{-2}	7625	2.81	2.70	2.47
	0.5	9.35×10^{-2}	7413	2.81	2.70	2.47
	4	9.72×10^{-2}	7131	2.81	2.70	2.46
	20	9.93×10^{-2}	6980	2.81	2.70	2.45
	20	10.4×10^{-2}	6665	2.81	2.70	2.45
	20	11.9×10^{-2}	5825	2.81	2.70	2.45
	50	9.78×10^{-2}	7087	2.82	2.70	2.42
	100	11.7×10^{-2}	5924	2.83	2.70	2.39
	140	15.3×10^{-2}	4530	2.84	2.70	2.36
100	0.5	5.55×10^{-1}	1249	2.83	2.68	2.46
	2	6.11×10^{-1}	1134	2.83	2.68	2.46
	4	6.33×10^{-1}	1095	2.83	2.68	2.46
	10	7.26×10^{-1}	955	2.83	2.68	2.45
	20	7.10×10^{-1}	976	2.84	2.68	2.44
	20	7.33×10^{-1}	946	2.84	2.68	2.44
	20	7.70×10^{-1}	900	2.84	2.68	2.44
	50	7.60×10^{-1}	912	2.85	2.68	2.41
	100	7.64×10^{-1}	907	2.86	2.68	2.37
	140	1.0	693	2.87	2.68	2.34
120	0.5	3.2	217	2.88	2.67	2.47
	0.5	3.4	204	2.88	2.67	2.47
	2	3.8	181	2.88	2.67	2.47
	4	3.5	198	2.88	2.67	2.46
	20	3.4	204	2.89	2.67	2.44
	20	3.8	181	2.89	2.67	2.44
	20	3.8	182	2.89	2.67	2.44
	50	4.0	172	2.90	2.66	2.41
	100	4.0	181	2.91	2.66	2.36
	140	5.2	133	2.92	2.66	2.33
Hydrolysis rate constants obtained in the HDAC						
T [°C] ± 1 [°C]	**P [MPa] ± 20 [MPa]**	**k [× 10^{-3} s^{-1}] ± 10%**	**$t_{1/2}$ [s] ± 10%**	**l_1+q**	**l_2+q**	**l_3+q**
80	0.1	7.51×10^{-2}	9762	2.81	2.70	2.47
	90	1.04×10^{-1}	6664	2.81	2.70	2.39
	584	2.2×10^{-1}	3150	n.a.	n.a.	n.a.
	934	6.3×10^{-1}	1100	n.a.	n.a.	n.a.
100	116	4.8×10^{-1}	1444	2.83	2.68	2.35
	365	5.9×10^{-1}	1175	2.84	2.68	2.22
	508	7×10^{-1}	990	n.a.	n.a.	n.a.
	1016	2	347	n.a.	n.a.	n.a.
	1666	6.4	108	n.a.	n.a.	n.a.
120	176	4.6	126	2.88	2.67	2.31
Hydrolysis rate constants at Psat obtained in HDAC						
T [°C] ± 1 [°C]	**P [MPa]**	**k [× 10^{-3} s^{-1}]**	**$t_{1/2}$ [s]**	**l_1+v**	**l_2+v**	**l_3+v**
100	0.1	5.5×10^{-1} ± 10%	1260 ± 10%	2.83	2.61	2.46
Moeller et al. (2022)						
80	0.05	6.1×10^{-2} ± 0.0036	11304 ± 63	2.81	2.63	2.47
100	0.1	5.8×10^{-1} ± 0.089	1164 ± 0.29	2.83	2.61	2.46
120	0.2	4.3 ± 0.012	143 ± 0.01	2.88	2.61	2.47
Hydrolysis rate constants of D_2O solutions obtained in the autoclave						

T [°C] ± 5 [°C]	P [MPa] ± 0.2 [MPa]	k [× 10^{-3} s^{-1}] ± 10%	$t_{1/2}$ [s] ± 10%			
80	20	0.10	6931	n.a.	n.a.	n.a.
100	10	0.85	815	n.a.	n.a.	n.a.
	20	0.97	714	n.a.	n.a.	n.a.
	20	0.89	778	n.a.	n.a.	n.a.
	20	0.90	770	n.a.	n.a.	n.a.
	20	0.90	770	n.a.	n.a.	n.a.
	50	0.70	990	n.a.	n.a.	n.a.
120	20	3.95	175	n.a.	n.a.	n.a.
	20	4.41	157	n.a.	n.a.	n.a.

To the best of our knowledge, only Leibrock et al. (1995) have determined the hydrolysis rate constants of ATP at elevated pressures up to 220 MPa. A systematic difference by a factor of approximately two to our data is clearly visible (Figure 5) even though the rate constants of our study are in the same order of magnitude as those of Leibrock et al. (1995). Leibrock et al. (1995) used nuclear magnetic resonance (NMR) to measure ATP concentrations in quenched D_2O solutions derived from quenched experiments. To ensure comparability with Leibrock et al. (1995), we carried out 9 hydrolysis experiments in the autoclave in D_2O at 80 °C, 100 °C and 120 °C at 10 MPa, 20 MPa and 50 MPa (Figure 5, Table 4). Eight rate constants as a function of pressure were reported by Leibrock et al. (1995) in Figure 5 (in reference) in a relative manner normalized to the value at 10 MPa. These relative values were taken from the graphs and converted to absolute values based on the rate constant at 100 MPa and pD 5 in Leibrock et al. (1995) Figure 2 (in reference). The pH was corrected to pD 3.38 using the relation shown in Leibrock et al. (1995), Figure 4 therein (in reference). Figure 5 summarizes the comparison of these two studies. The rate constants from Leibrock et al. (1995) show an increase in pressure by a factor of ca. 1.4 with a maximum between 120 MPa and 140 MPa. At higher pressures up to 220 MPa, the rate constants measured by Leibrock et al. (1995) decrease to a value at up to the pressure of 220 MPa that is below the initial value at 10 MPa. Our values for both the D_2O and H_2O systems also demonstrate an increasing trend up to 140 MPa by a similar factor of roughly 1.4. We obtained only few measurements of the ATP hydrolysis rate constants between 140 and 220 MPa and thus could not compare our data well with those of Leibrock et al (1995) in this pressure range.

We note that our data show that the ATP hydrolysis rate constants determined in D_2O are indistinguishable within error from those obtained in H_2O and that the difference in solvent is unlikely to be the explanation for the differences between our data and those of Leibrock et al (1995). However, our data at higher pressure from the HDAC do not indicate any decrease or a minimum in the pressure dependence. The rapid increase of the rate constant at pressures above 500 MPa raises the intriguing question of whether there is a progressive change or two not yet identified abrupt changes between 500 MPa and 1000 MPa, and between 1000 MPa and 1600 MPa. Currently, the data are consistent with both possibilities, therefore, more data on rate constants at high pressures are needed to address this question.

Figure 5 compares three sets of *in situ* rate constants for the hydrolysis of ATP under three different conditions: at vapor-saturated conditions in the HDAC, at isochoric conditions in the HDAC, and at isobaric conditions in the autoclave. The investigated pressure range of 0.5 MPa to 140 MPa in the autoclave is too narrow and scattered to derive a distinct trend. In the HDAC at isochoric conditions, the rate constants exhibit similar progressive trends at 80 °C and 100 °C. Assuming that the hydrolysis rate changes continuously with pressure, the data were fitted

with an empirical power law allowing only positive integers in the exponent. The data were best fitted by a power law of the following format (Eq. 4):

$$k(P) = k_0 + a * P^3 \qquad \text{Eq. 4}$$

where k(P) is the rate constant as a function of pressure (P), k_0 is the calculated rate constant at P=0 MPa and a is a parameter. The results of the fits and their respective standard deviations are as follows: $k_{0,80\,°C}=1.0 \times 10^{-4}\ s^{-1} \pm 0.1 \times 10^{-4}\ s^{-1}$ and $a_{0,80\,°C} =6.3 \times 10^{-13} \pm 0.69 \times 10^{-13}$ for the dataset at 80 °C and $k_{0,100\,°C}=5.0 \times 10^{-4}\ s^{-1} \pm 0.34 \times 10^{-4}\ s^{-1}$ and $a_{0,100\,°C} =1.34 \times 10^{-12} \pm 0.12 \times 10^{-12}$ for the dataset at 100 °C. The chi-square values (χ^2) are 0.19 for the fit of the power laws at 80 °C and 0.93 for the fit at 100 °C (Eq. 5):

$$\chi^2 = \sum\left(\frac{k_{expected} - k_{measured}}{\sigma_{1,measured}}\right)^2 \qquad \text{Eq. 5}$$

where $k_{expected}$ is the rate constant from the fitted line, $k_{measured}$ are the measured rate constants and $\sigma_{1,\,measured}$ is the first standard deviation of the measured rate constants. Ideally, a chi-square value equal to the number of fitted points would indicate a perfect fit for the weighted coefficients of the data. A chi-square value lower than the number of fitted points suggests potential overfitting of the data or too large uncertainties. However, in a first instance, these fits adequately capture the trends, given the limited number of data points. Th error propagation of the fit parameter results in a standard deviation of 15% for the fitted line at 80 °C and 11% at 100 °C.

The highest experimental pressure at which a rate constant could be obtained was 1670 MPa at 100 °C. This rate constant is about 6.4×10^{-3} 1 s^{-1}, which corresponds to a half-life of 108 s. That half-life at 1670 MPa and 100 °C is 25 s shorter than the value reported by Moeller et al. (2022) at Psat and 120 °C. In experiments at 100 °C and pressures above 2000 MPa, only AMP in solution was detected. Thus, (near) complete hydrolysis of ATP to AMP took place within about 30 s, after heating was stopped and before the very Raman spectrum of the solution was acquired. In these experiments, we observed nucleation and growth of crystals (Figure 6).

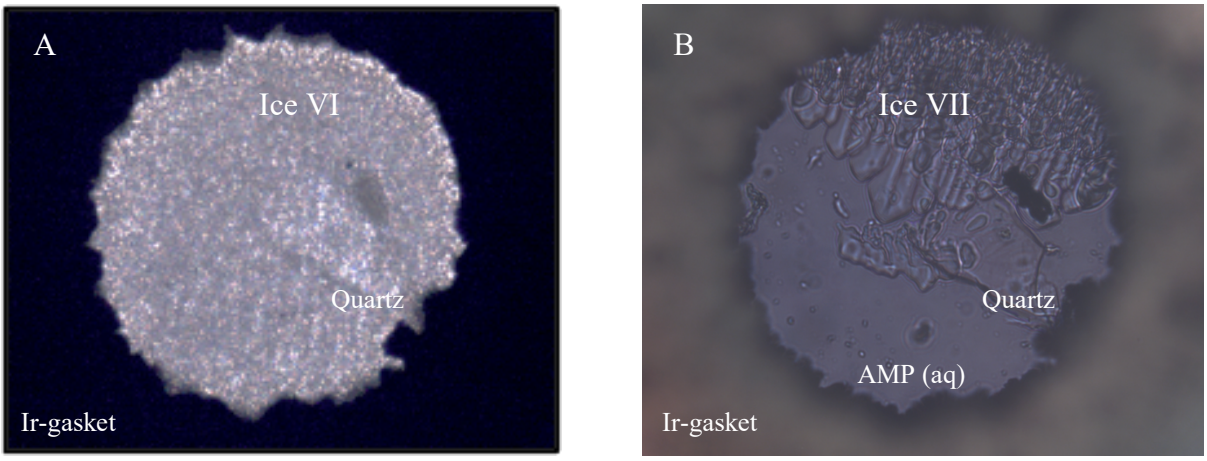

Figure 6: View of the sample chamber of the HDAC showing the experiment at the highest pressure. A: Ice VI and quartz at 2.06 GPa and 26 °C. B: Ice VII, AMP solution, and quartz at 2.3 GPa and 100 °C. Quartz was used as a Raman spectroscopic pressure sensor. The initial diameter of the sample chamber was 300 µm.

A Raman spectrum of the solid phase indicated Ice VII at 100 °C and 2.3 GPa (Figure 7). The identification is based on the OH stretching band shape (Walrafen et al., 1984). At 26 °C and 2.06 GPa, the Raman spectrum of the solid phase was superimposed by luminescence of the AMP solution, preventing unambiguous identification. Upon heating, this solid phase transformed to Ice VII at about 92 °C, which suggests that it was most likely Ice VI.

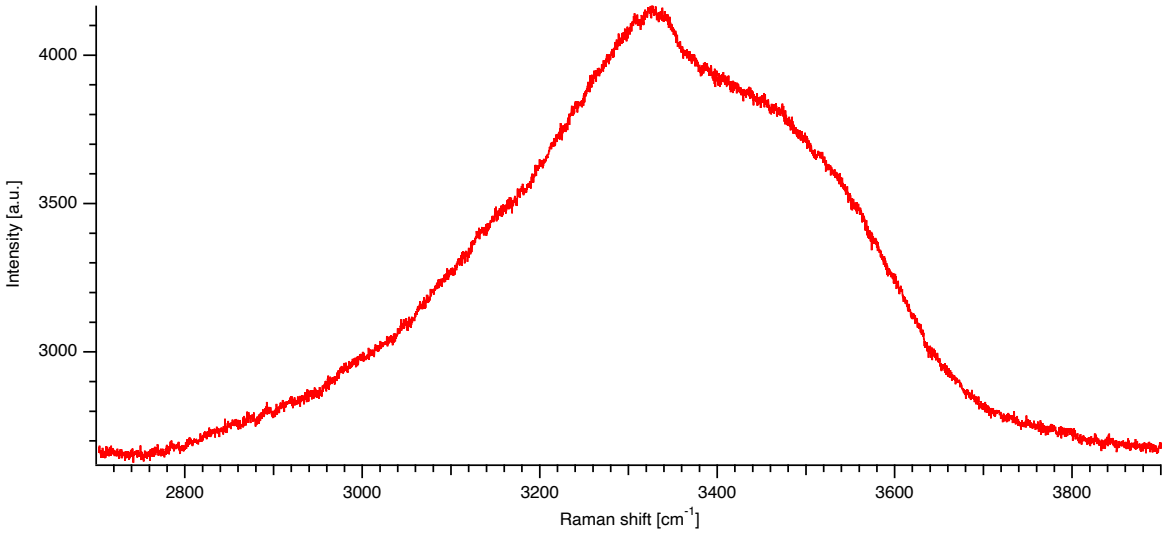

Figure 7: Raman spectra of the solid phase at 100 °C and 2.3 GPa identified as Ice VII after Walrafen et al. (1984). The raw data are available in the Data Availability section ([dataset] Moeller et al., 2024).

4. Discussion

4.1. Data quality

The complementary application of the HDAC and an autoclave has yielded insights into the kinetic properties of ATP hydrolysis at elevated temperatures and pressures up to 1670 MPa that were previously unattainable. In the overlapping pressure range, the hydrolysis rate constants of both setups deviate by an average factor of 1.2 ± 0.3. However, in both datasets, a similar relative increase by a factor of 1.34 ± 0.07 is shown between 0.1 MPa to 100 MPa and 0.1 MPa to 90 MPa, respectively.

The observed discrepancy between the two methods may be attributed to the applied laser intensities of 32 mW and 80 mW in the HDAC and autoclave, respectively. It is improbable that visible light absorption occurs in colorless solutions. Moreover, any minor heating induced by the laser would likely be homogenized by convection in the reaction cells. Nevertheless, it is not possible to completely rule out the possibility of heating nor of direct photon-molecule reactions induced by the laser. Therefore, measurements of ATP-H_2O sample solutions were repeated at 20 MPa and 100 °C in the autoclave, utilizing both laser intensities of 20 mW and 80 mW for comparison. A reduction in laser intensity by 60 mW resulted in a 20% to 25% decrease in the fitted values of the hydrolysis rate constants. The considerably lower signal-to-noise ratio at 20 mW laser power resulted in poorer counting statistics of the spectra, which then led to a larger error in the ATP/ADP estimates, as documented by the larger scatter of the data points (Figure 8). The poorer quality of the data likely contributed to the apparent decrease of the hydrolysis rate by 20% to 25%.

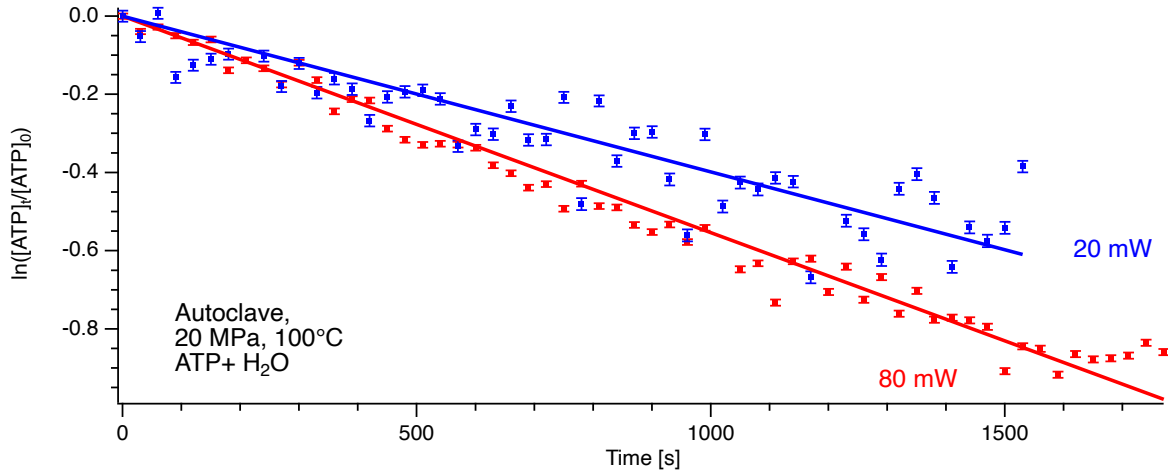

Figure 8: Linear fits of ln([ATP]$_t$/[ATP]$_0$) vs. Time for measurements with laser intensities of 20 mW and 80 mW. The measurements were taken in the autoclave at 20 MPa and 100 °C for solutions of ATP-H_2O. The raw data are available in the Data Availability section ([dataset] Moeller et al., 2024).

This potential photo-stimulatory effect presents an intriguing phenomenon. In the field of biochemistry, a multitude of experiments involve the use of "caged" molecules. These molecules are rendered inactive through chemical modification (Kaplan and Somlyo, 1989) until they are activated by UV light with a wavelength greater than 300 nm (Mayer and Heckel, 2006). It is noteworthy that the term "caged molecules" was initially coined in the context of experiments concerning ATP hydrolysis (Kaplan et al., 1978). Although this technique is well described in the literature, a photo-stimulation of the ATP hydrolysis has not yet been reported, and further investigation may be needed.

The discrepancy between the rate constants determined in the HDAC and in the autoclave observed at 80 °C may also be attributed to the precision of the temperature measurement in the autoclave itself. Temperature measurements in the HDAC are accurate to within 1 °C (Schmidt and Chou, 2012). Temperature measurements of the autoclave are more complex due to the large sample chamber, which results in the existence of temperature gradients between the heater and the sample chamber. Heat transfer is ensured by convecting helium at high pressure. Currently, the estimated accuracy of the setup is approximately 5 °C. This 5 °C deviation could plausibly contribute to the observed difference in the datasets.

Moreover, the minor discrepancies between the HDAC data, HDAC at Psat data (Moeller et al 2022) and the autoclave experiments may be attributed to the three distinct chemical systems involved. The following chemical systems were considered: ATP in aqueous solution (l_1, l_2 and l_3, in table 3), ATP in aqueous solution coexisting with a vapor phase (l_1+v, l_2+v and l_3+v, in table 3) and ATP in aqueous solution and a quartz grain in the HDAC (l_1+q, l_2+q and l_3+q, in table 3). In order to test possible effects, the concentrations of the chemical species were calculated and the pH was utilized as an indicator for changes in the solution in the three cases (Table 4). For a single aqueous phase, a progressive decrease in pH from 2.8 to 2.7 and 2.47 was observed as ATP hydrolysis progressed. The calculated differences in pH due to the presence of an additional vapor phase or a quartz grain are within the error of calculations and thus considered insignificant.

In conclusion, the disparity in hydrolysis rates of ATP observed between the HDAC and autoclave experiments is not attributable to differences in system composition. A 20% to 25%

reduction in the fitted value of ATP hydrolysis rate constants was observed in the autoclave when laser intensity was reduced from 80 mW to 20 mW. A number of potential explanations for this discrepancy exist, including a lower signal-to-noise ratio, laser illumination effects or systematic temperature differences between the setups. It is important to note that this difference falls within the estimated 5 °C uncertainty of temperature calibration within the autoclave. Moreover, the small offsets between HDAC data and low-pressure data in the presence of a vapor phase (Moeller et al., 2022) are also likely due to subtle temperature calibration or laser illumination effects, which would be interesting to determine in future studies.

4.2. Effect of temperature on rates of ATP hydrolysis at isobaric conditions

The temperature dependence of the kinetics of a chemical reaction is evaluated using the Arrhenius equation (Eq. 6) where R=8.314 J K^{-1} mol^{-1} is the ideal gas constant, T the temperature [K] and A is the pre-exponential or frequency factor [s^{-1}]. An Arrhenius plot relates the temperature, apparent activation energy and rate constants graphically (Figure 9). The term apparent activation energy is used since the solutions were unbuffered in pH which causes pH variations between given temperatures due to different repartition of ATP species e.g., ATP^{4-}, $HATP^{3-}$, H_2ATP^{2-} (Moeller et al., 2022).

$$lnk = \frac{E_a}{R} * \frac{1}{T} + A \qquad \text{Eq. 6}$$

The data at pressures between 0.5 MPa and 140 MPa plot on a straight line, indicating a constant reaction mechanism between 80 °C and 120 °C. The apparent activation energy, E_a, is not significantly different at 4 MPa and 140 MPa (respective values 104 kJ mol^{-1} ± 30 kJ mol^{-1} at 0.5 MPa to 101 kJ mol^{-1} ± 30 kJ mol^{-1} at 140 MPa). The pre-exponential factor, A, ranges between 25.6 ± 9.4 and 28.5 ± 9.6. The average activation energy is 104.3 kJ/mol ± 30 kJ/mol and the pre-exponential factor is 26.5 ± 9.5. A potential effect within this pressure range on the hydrolysis of ATP is insignificant given these uncertainties. Moeller et al. (2022) reported an activation energy of 122.7 kJ mol^{-1} ± 4.4 kJ mol^{-1} at Psat. The uncertainty in activation energy was based on the square root of the initially fitted integral, which was propagated throughout their study. A new fit of the data of Moeller et al. (2022) with a standard deviation of 10% yielded an activation energy of 122 kJ mol^{-1} ± 30 kJ mol^{-1} and a pre-exponential factor of 32.1 ± 9.8 for their data at pH 3 and Psat. Additionally, Moeller et al. (2022) reported rate constants at pH 7. If we re-fit also these data with uncertainties of 10%, the activation energy is 124 kJ mol^{-1} ± 32 kJ mol^{-1} and the pre-exponential factor is 32.2 ± 10.3. The discrepancy in the activation energies reported by Moeller et al. (2022) and the refitted values is likely due to a mistake, i.e., transposed numbers in the gas constant, 8.13, which was used instead of 8.31. The effect of this number transposition appears to be relatively minor, given the inherent uncertainties. However, at vapor saturation and 80 °C, ATP hydrolysis rates are found to be slower than those without vapor phase, respectively. At 100 °C the rate constants are almost equal and at 120 °C the constants at Psat are larger than those at elevated pressure as discussed above. This

suggests a stronger temperature dependency for the hydroylsis rates in the presence of vapor than in a single liquid.

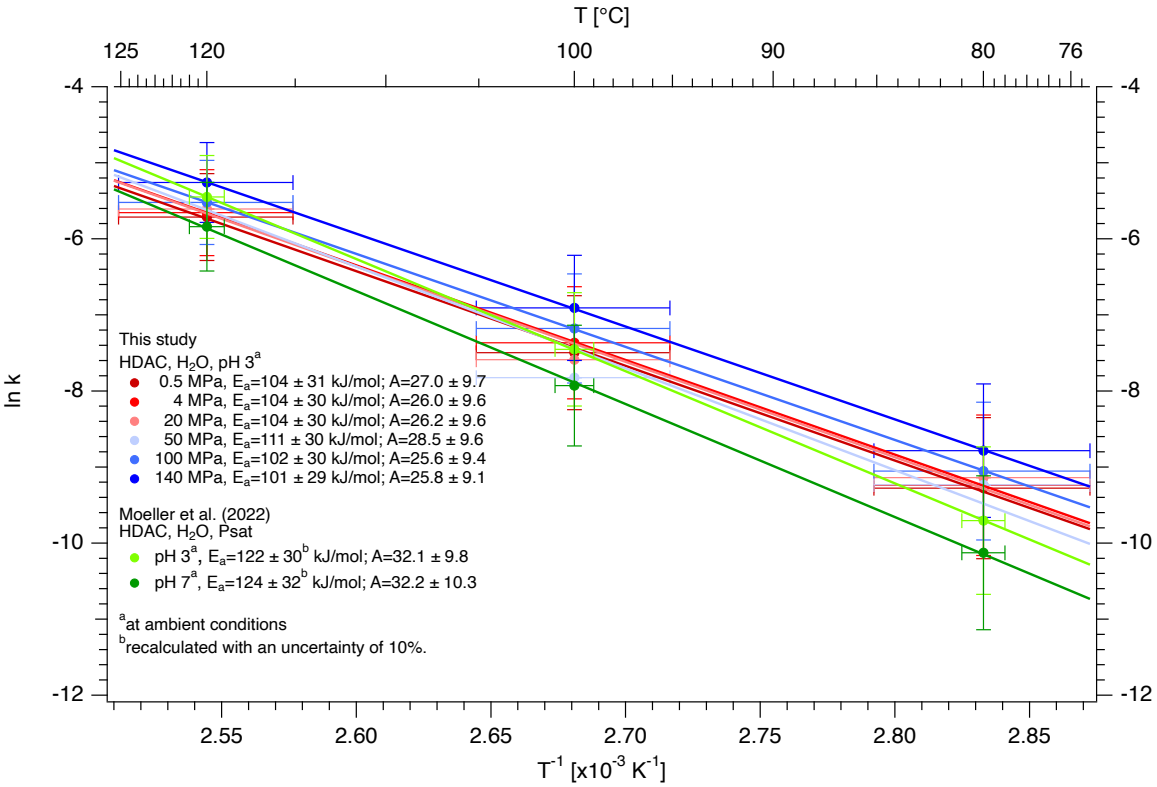

Figure 9: Arrhenius plot of the isobaric hydrolysis rate constants in comparison to kinetic data of Moeller et al. (2022) and Daniel et al. (2004).

At pressures above 140 MPa, data on ATP hydrolysis rates are available only at two temperatures, 80 °C and 100 °C, for each pressure. In this case, the results from the fitted power law functions (Eq. 3, 4) can be used in a first approximation to provide an estimate of isobaric activation energies ($E_{a,extrapolated}$), which have been extrapolated in [J] according to the following equation:

$$E_{a,extrapolated} = \frac{\ln\, k(P)_{100\,°C} - \ln\, k(P)_{80\,°C}}{\left(\frac{1}{373} - \frac{1}{353}\right)} * R \qquad \text{Eq. 7}$$

where k(P) is the calculated rate constant from Eq. 4 at 80 °C and 100 °C at a given pressure and R is the universal gas constant. This estimation yields an activation energy of 88 kJ mol^{-1} ± 16.4 kJ mol^{-1} at 1 MPa (Figure 10), which differs by approximately 20% from the calculated values determined in the autoclave. This discrepancy may be acceptable given that only two isotherms were available from the HDAC runs, which are based on eight individual experimental loadings. Only above 150 MPa to 200 MPa is there a substantial decrease in the extrapolated activation energy, which reaches a value of about 42 kJ mol^{-1} at 1700 MPa. This observation lend support to the observation that the changes in activation energy and thus, in the reaction mechanism between 0.5 MPa and 140 MPa are insignificant.

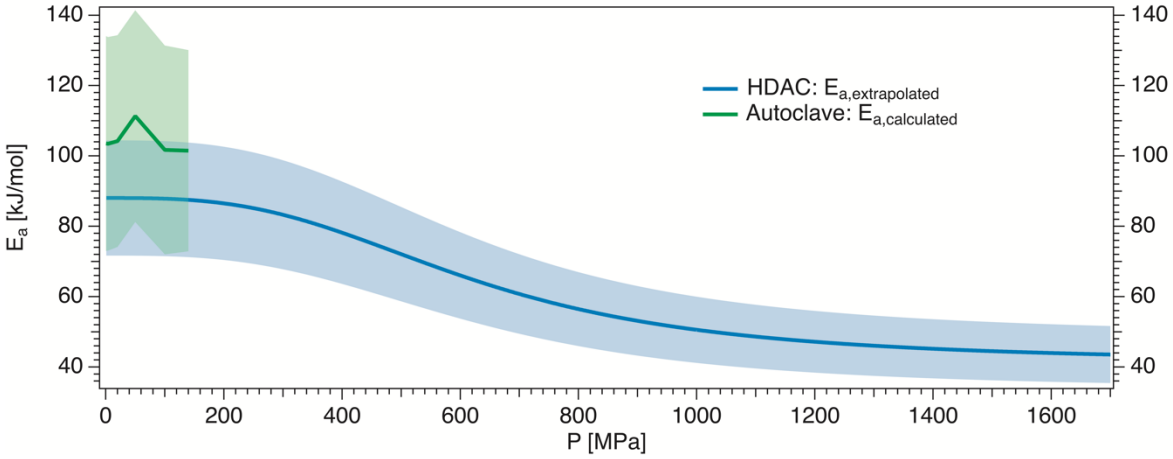

Figure 10: Calculated activation energies from autoclave experiments and extrapolated activation energies from fitted power laws of HDAC data as functions of pressure.

4.3. Effect of pressure on rates of ATP hydrolysis at isothermal conditions

To our knowledge the only other study investigating the pressure effect on the hydrolysis rate constant of ATP is that of Leibrock et al. (1995). They analyzed samples quenched from high temperatures and pressures. The concentration was determined with subsequent NMR analysis, which is a highly accurate and precise analytical tool. Replacement of H_2O by D_2O may result in slowing down any reaction involving breaking of hydrogen bonds (Westheimer, 1961). As illustrated in Figure 4, the rate constants determined by Leibrock et al. (1995) in D_2O are lower by roughly 50 % lower than those measured in H_2O in the present study. However, the rate constants obtained here for the ATP-D_2O system (Figure 5 and 6) are within the uncertainty of the data for H_2O. Therefore, a kinetic isotope effect alone, as proposed by Moeller et al. (2022), would not explain the slightly slower ATP hydrolysis rates of Leibrock et al 1995 (Figure 6). The enhanced decomposition of ATP under high laser power could account for an increase in the ATP hydrolysis rate constant of up to 25% in some of our experiments as previously discussed. Furthermore, it is important to consider the potential impact of artifacts due to quenching and subsequent analysis in *ex situ* studies. Quenching may lead to artifacts due to back reactions and other alterations of the species' concentrations after quenching and depressurization. It is possible that the data of Leibrock et al. (1995) may have been affected by such effects. However, tests with solutions at ambient conditions as well as extrapolation of data here indicate that any reaction at ambient conditions will be extremely sluggish, making it unlikely that a change in concentration between the quench of the run and the NMR measurement would occur. The only significant differences between the two studies are the total concentrations of ATP, which were approximately ten times higher in this study, and the sample volume, which was approximately twenty-five times larger in Leibrock et al. (1995). However, the two datasets agree in terms of a relative increase in the rate constants up to 120 MPa to 140 MPa by a factor of approximately 1.4. A decrease in the ATP hydrolysis rate constants was observed by Leibrock et al. (1995) between 140 MPa and 220 MPa. However, rate constants in this pressure range could not be determined, as the autoclave was unable to reach these pressures. The application of the HDAC between 140 MPa and 220 MPa is challenging and results in uncertainties of 30 MPa due to the low resolution and sensitivity of quartz as a pressure indicator in this range. Beyond the pressure range studied by Leibrock et al. (1995), we observed

a continuous increase of the ATP hydrolysis constant with pressure above 400 MPa. In future studies, it would be beneficial to connect those observations by obtaining additional data points between 150 MPa and 400 MPa.

The effect of pressure on reaction rates depends on the reaction and the activation volume ($V^{\#}$). Le Châtelier's principle postulates that an increase in pressure will result in a shift of the chemical equilibrium towards the state with a smaller volume. Transferred to kinetic para-meters according to transition state theory, it implies that processes for which the transition states have the smallest volumes are the fastest (e.g., Mohana-Borges et al., 1999; Jebbar and Oger, 2010). The activation volume, is defined by (e.g., Kelm and Palmer, 1977):

$$V^{\#} = -RT\ \frac{dln\ k}{dP} \qquad \text{Eq. 8}$$

where R is the universal gas constant. The activation volume of ATP hydrolysis can be determined for the dataset of single-phase aqueous high-pressure experiments in and the autoclave and the HDAC by using the Eq. 8. In the autoclave, the determined values of $V^{\#}$ for the pressure range of 0.5 MPa to 140 MPa are -8.4 $cm^3\ mol^{-1} \pm 2\ cm^3\ mol^{-1}$ at 80 °C, -8.7 $cm^3\ mol^{-1} \pm 2\ cm^3\ mol^{-1}$ at 100 °C and -8.1 $cm^3\ mol^{-1} \pm 2\ cm^3\ mol^{-1}$ at 120 °C. In the HDAC, $V^{\#}$ is -5.5 $cm^3\ mol^{-1} \pm 1.5\ cm^3\ mol^{-1}$ for 90 MPa to 934 MPa at 80 °C and -6.3 $cm^3\ mol^{-1} \pm 4.1\ cm^3\ mol^{-1}$ for 116 MPa to1166 MPa at 100 °C. On average, $V^{\#}$ is 7.4 ± 0.82 $cm^3\ mol^{-1}$. Leibrock et al. (1995) reported a value of -15 ± 4 $cm^3\ mol^{-1}$ over a pressure range between ca. 10 MPa and 120 MPa. Based on the literature cited therein, Leibrock et al (1995) suggested that values between -8 $cm^3\ mol^{-1}$ and -15 $cm^3\ mol^{-1}$ are consistent with a mechanism of anhydride and ester hydrolysis (A_{AC} 2-mechanism). Asano and Noble (1978) distinguished the activation volume for ester hydrolysis between -10 $cm^3\ mol^{-1}$ and -15 $cm^3\ mol^{-1}$ for basic solutions and greater than -10 $cm^3\ mol^{-1}$ for acidic solutions, which aligns with our findings. In the context of ester hydrolysis, protonation of the phosphate group by H^+ precedes a nucleophilic attack of H_2O (Figure 11).

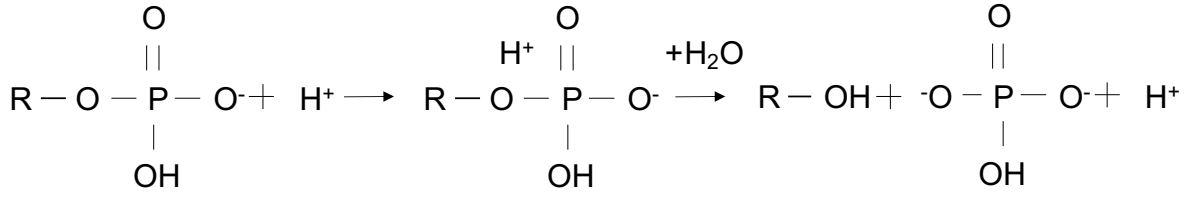

Figure 11: Reaction scheme of the anhydride and ester hydrolysis after Leibrock et al. (1995).

Leibrock et al. (1995) proposed that the nucleophilic attack of water represents the limiting factor of hydrolysis at low pressures and the protonation reaction becomes rate limiting at pressures above 120 MPa. It can be postulated that the negative activation volumes and thus enhancement of ATP hydrolysis rates with pressure may be related, at least in part, to the fact that the ionization product of water increases with pressure. This implies that the neutral pH of water decreases as pressure increases. For instance, isothermal compression of pure water at 100 °C would result in a shift of the pK_w from 12.25 at 0 MPa to 11.94 at 100 MPa and to 11.02 at 500 MPa. This would consequently lead to a shift in the neutral pH of water from 6.1 to 6 and to 5.5. To test the hypothesis that an increased autoprotolysis of water with increasing

pressure affects ATP hydrolysis, the pH was calculated in thermodynamic equilibrium of ATP solutions containing ATP, ADP, AMP, and inorganic phosphate groups (Table 4). The calculated pH_P values for solutions of 0.1 mol/l ATP at equilibrium conditions for the three species are shown in Figure 12. The calculations predict a significant decrease in the pH value with increasing pressure for a given temperature. The changes in pH for solutions of 0.01 mol/l ATP are within 0.1 to 0.3 per 500 MPa. Therefore, the general decrease with increasing pressure is consistent with the enhancement of the hydrolysis rate with decreasing pH, as reported by Leibrock et al. (1995).

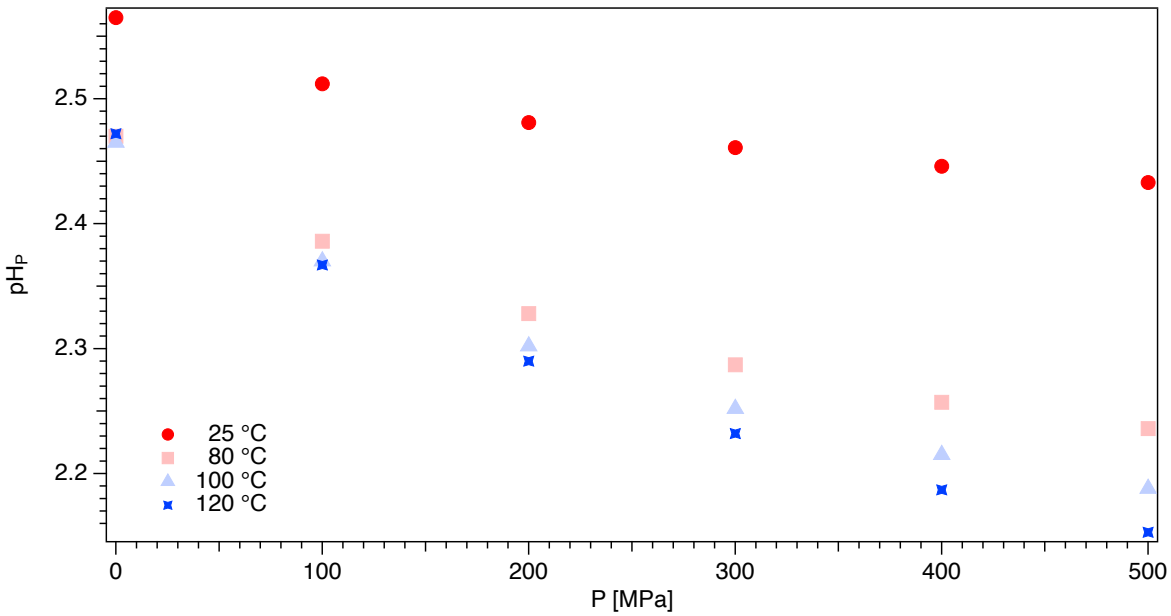

Figure 12: The modelled pH of 0.1 mol/l ATP solutions without gaseous species at equilibrium conditions, here solution l_1 (see Table 3), as a function of pressure at 25 °C, 80 °C, 100 °C, and 120 °C. The absolute pH values are available in the Data Availability section ([dataset] Moeller et al., 2024).

It can be concluded that elevated pressure may increase the catalyzing effect of hydronium ions on the hydrolysis reaction. However, this model does not explain the decrease in ATP hydrolysis rate observed by Leibrock et al. (1995) above 120 MPa and up to 220 MPa. To resolve this discrepancy, it is necessary to obtain more *in situ* data of ATP hydrolysis in this pressure range.

Above 2000 MPa and 100 °C, no rate constants were determined as the hydrolysis rate was below the temporal resolution of our experimental setup with the hydrothermal diamond anvil cell. However, it is evident that the complete abiotic hydrolysis of ATP to AMP must have occurred within the initial 30 s of heating and 20 s of the very first spectrum acquisition, as only AMP was detectable. To evaluate this observation, we can extrapolate with Eq. 4 the hydrolysis rate of ATP to 2000 MPa and 100 °C. The rate is approximately 0.1 s^{-1} with a corresponding half-life of few seconds. Thus, our minimum measurement time of the first spectra of 50 s would encompass several half-lives under such conditions. At this point in time, the remaining concentration of ATP was below 0.001 mol/l, which is below the detection limit of approximately 0.005 mol/l.

4.4. Implications for the limits of metabolic pathways

In order to contextualize the abiotic hydrolysis of ATP data within the biological realm, it is interesting to compare them with ATP turnover times that have been measured in

microorganisms (see Bains et al., 2015). The average pool turnover rate is defined as the quantity of material that is turned over per unit of time in a biological system (Zilversmit, 1955). The average pool turnover rate of ATP for *Escherichia coli sp.* is 0.05 s^{-1}, while for *Bdellovibrio bacteriovorusis sp.* it is 0.13 s^{-1} at 28 °C (Gadkari et al., 1976). For some *Streptococcus mutans sp.,* these rates are up to 1.5 s^{-1} at 37 °C (Fukui et al., 1988). It is important to note that these microorganisms are mesophiles and are not exposed to any extreme conditions, such as temperature or pressure, which might strongly affect the turnover times. To our best knowledge, these have not yet been measured in extremophiles.

In a first approximation and neglecting other potentially very important biological effects, Moeller et al. (2022) used the Arrhenius relation to determine the temperature at which the hydrolysis rate equals to the pool turnover rate of 0.05 s^{-1} of *Escherichia coli sp.* and of 1.5 s^{-1} of *Streptococcus mutans sp.* by inserting them into the rearranged Arrhenius equation (Eq. 9):

$$T = \frac{\frac{E_a}{R}}{\left(ln\, k_{average\ pool\ turnover\ rate} - A\right)}. \qquad \text{Eq. 9}$$

Moeller et al. (2022) estimated that the maximum temperatures allowing cells to maintain their ATP pools were on average 145 °C ± 3 °C for *Escherichia coli sp.* and 195 °C ± 3 °C for *Streptococcus mutans sp.* For pH 3 and pH 7, the authors estimated an average tentative lower and upper temperature limit for ATP-supported metabolism to be 145 °C ± 3 °C and 195 °C ± 3 °C at Psat for pH 3 to 7. The authors' conclusion was that, with the exception of measuring ATP turnover times in hyperthermophilic organisms, abiotic destabilization of ATP does not appear to be the primary factor determining the currently observed temperature limit of life. The lower temperature limit of ATP is 144 °C ± 57 °C and the upper temperature limit is 189 °C ± 75 °C at pH 3 and Psat, when using the refitted parameters with an uncertainty of 10% for the data reported above. In the present study, the average temperature limits for the single fluid phase are 152 °C ± 69 °C and 207 °C ± 95 °C at pH 3, based on a similar comparison with the parameters.

Similarly, by rewriting Eq. 4 as Eq. 10 and inserting the pool turnover rates of *Escherichia coli sp.* and of these *Streptococcus mutans sp.,* a lower and an upper pressure limit can be estimated at 80 °C (Equation 10) and at 100 °C, respectively.

$$P = \sqrt[3]{\frac{k_{average\ pool\ turnover\ rate} - k_{0,80\,°C}}{a_{80\,°C}}} \qquad \text{Eq. 10}$$

The estimated lower pressure limits are of 4.3 GPa ± 0.7 GPa at 80 °C and 3.3 GPa ± 0.3 GPa at 100 °C, while the upper pressure limits are 13 GPa ± 2 GPa at 80 °C and 10 GPa ± 1 GPa at 100 °C. Remarkably, the upper pressure limits are almost a magnitude higher than the maximum pressure of 1.6 GPa reached in our experiments. Such estimates are far beyond the phase boundary of liquid water and Ice VII, which is between 2.2 GPa and 2.8 GPa at temperatures from 80 °C to 120 °C (Bridgman, 1937). Figure 15 shows the phase diagram of water as a function of pressure and temperature (after Eisenberg and Kauzmann 1969; Guildner et al., 1976; Petrenko and Whitworth, 1999; IAPWS, 2011; Journaux et al., 2020), including the lower and the upper temperature limit of the ATP hydrolysis obtained in this study and by

Moeller et al. (2022). Interestingly, the comparison to pool turnover rates suggests that ATP is kinetically stable enough to sustain known metabolic pathways across the entire pressure range of liquid water, at least up to 100 °C.

These lower and upper P-T-limits can help to understand the P-T-conditions compatible with ATP-involving metabolic pathways in extreme environments, both on Earth and on other planets. Figure 15 provides information about extreme conditions in terrestrial settings adapted from Table 2 and 5 in Merino et al. (2019) and the tolerance ranges of *Methanopyrus kandleri sp.* (Takai et al., 2008) and *Thermococcus piezophilus sp.* (Dalmasso et al., 2016). This graphic compilation suggests that, from the necessarily limited point of view of comparing the pool turnover rate with the kinetic stability of ATP, metabolic pathways may be possible up to pressures of a few GPa.

Earth's subsurface is subject to high-pressure and temperature environments (Merino et al., 2019; Figure 13). The known deep biosphere is estimated to span only an average of the first 5 km of the Earth's crust, based on a geothermal gradient of 25°C/km to 30 °C/km and a crustal pressure gradient of 30 MPa/km with temperature and pressure limits of 122 °C and 130 MPa to 150 MPa (Oger and Jebbar, 2010). This environment is believed to host 15% Earth's total biota (Bar-On et al., 2018). Notably, these thresholds are considerably lower than the estimated kinetic stability range of ATP (Figure 13), suggesting that abiotic hydrolysis of ATP is not a limiting factor for known life forms. Finally, this raises the intriguing question of whether life could in principle exist deeper into the subsurface. Plümper et al. (2017) and Sharma et al. (2002), attempted to address this issue. Plümper et al. (2017) discovered organic matter encapsulated in rock clasts in an oceanic serpentinite mud volcano in the vicinity of a subduction zone forearc. In diamond anvil cell experiments, Sharma et al. (2002) reported the viability of *Shewanella oneidensis sp.* at 1.6 GPa and 25 °C (Figure 13). While both studies attracted considerable attention, they lacked definitive evidence to support their hypotheses. In particular, Sharma et al. (2002) was merely measuring an abiotic enzymatic reaction (Yayanos, 2002). We may conclude from the limited perspective of kinetic stability of ATP, should life exist beyond the notion of life, ATP hydrolysis could still be a suitable energy system in living cells.

It is important to note that physical extremes, such as temperature and pressure, can affect the intra- and extracellular environment of a microorganism. In contrast, chemical extremes, such as pH and salinity, primarily affect the habitat of an organism. Extremophiles invest a significant quantity of metabolic resources to maintain their intracellular environment at a neutral pH (e.g., Golyshina et al., 2006). Self-regulatory mechanisms, known as homeostasis, ensure internal stability and optimal functioning of vital processes (Cannon, 1929). Nevertheless, to avoid chemical crossover effects by bases and buffers, ATP solutions with only Na_2H_2ATP as an ion source were selected for this study. The pH-relation shown by Leibrock et al. (1995), which is supported by measurements of Moeller et al. (2022), indicates the rate constants at pH 3 should be halved in order to obtain an estimate for rate constants at pH 7. Based on the refitted Arrhenius parameter at pH 7 for the data of Moeller et al. (2022), the tentative

temperature limits shift consistently by 7 °C to higher temperatures. This shift is negligible, given that the estimated limits are already beyond the common notions of life, as discussed earlier.

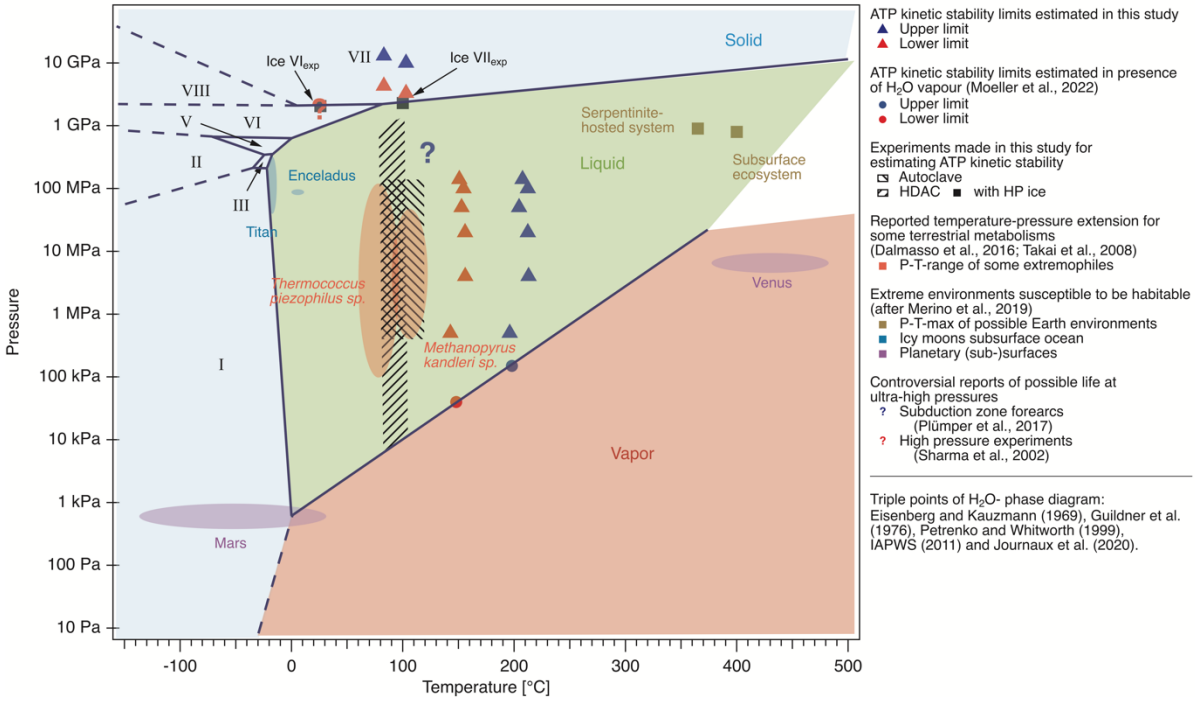

Figure 13: Estimated limits of ATP kinetic stability temperature-pressure field superimposed to the H_2O phase diagram, to possible environments for life and to experimental reports on living microorganisms.

The use of ATP's kinetic stability in aqueous solution as a proxy for the possibility of metabolism is an oversimplified approach. Metabolic pathways involve various interrelated processes, and ATP-involving reactions are just a few of them. In addition, extremophiles have developed mechanisms such as substrate channeling (e.g., Legrain et al., 1995) or metabolite substitution, in which ATP is replaced by ADP in certain metabolic processes (Kengen et al., 1995). The upper and lower P-T limits proposed here for the kinetic stability of ATP are based on the average ATP pool turnover rates measured in mesophilic organisms. Therefore, the model does not consider the necessity for extremophiles to maintain normal cell functioning while utilizing substantial quantities of metabolic resources to compensate for thermal damage and cell integrity (Beulig et al., 2019). Additionally, this approach on the abiotic side also entails certain simplifications that warrant further investigation. For instance, the kinetic stability of ATP that were measured is based on chemical systems with only Na^+ and H^+ ions as counterions. It is well established that other ions, in particular Mg^{2+}, exert a significant influence on the reaction kinetics of ATP hydrolysis.

Furthermore, the approach could be greatly enhanced by a comprehensive investigation of the photostimulatory effect on ATP hydrolysis and the determination of rate constants at a neutral pH. Further insights could involve expanding our understanding of the biological turnover rates of ATP, particularly in extremophiles, and by considering the kinetic effects of abiotic ATP hydrolysis in the presence of ions such as Mg^{2+}. In light of these complexities, superimposing the kinetic stability field of ATP onto the phase diagram of water and correlating it with conditions under which life could potentially thrive will offer another perspective for discussing the potential distribution of terrestrial-like life forms in extreme environments.

5. Conclusion and outlook for the future

This study presents the first *in situ* determination of rate constants for the abiotic/non-enzymatic hydrolysis of ATP at high pressure and temperature. Thermodynamic calculations provide insights into the pH evolution of the ATP system under elevated temperature and pressure conditions. A first comparison of the abiotic hydrolysis rates to the biotic average pool turnover rates of ATP, as measured in mesophilic organisms, indicates that ATP hydrolysis may still be a viable energy system in living organisms. Furthermore, this comparison enables us to estimate lower and upper temperature and pressure limits for the kinetic stability of ATP. The result is a tentative kinetic stability field of ATP offering an interesting perspective on the potential extension of terrestrial and extraterrestrial life.

The application of different laser intensities may suggest that the hydrolysis of ATP is photo stimulated. This effect, which has not been yet reported in the literature, may require further quantification and consideration in future studies. Furthermore, the data currently available concern the kinetic properties of ATP in the presence of Na^+ and H^+ ions as counterions. However, divalent metal ions, in particular Mg^{2+}, form complexes with ATP that exert a significant influence on ATP hydrolysis kinetics. Further investigations aimed at quantifying the chemical effects of such complexes on the rates of abiotic hydrolysis of ATP would enhance our understanding of the kinetic stability field of ATP. In this context, the acquisition of new microbiological data on ATP turnover rates in extremophile microorganisms is of great importance.

Author statement after CRediT

Conceptualization: F. Guyot, M. Wilke
Methodology: C. Moeller, C. Schmidt, D. Testemale, M. Kokh
Formal analysis: C. Moeller, M. Wilke
Investigation: C. Schmidt, Testemale, C. Moeller, M. Kokh, M. Wilke
Resources: M. Wilke, C. Schmidt, D. Testemale
Writing – Original Draft: C. Moeller, M. Wilke
Writing – Review and Editing: F. Guyot, C. Schmidt, D. Testemale, M. Kokh
Visualization: C. Moeller
Project administration: M. Wilke
Funding acquisition: M. Wilke

Data Availability

Data are available through GFZ Data Services at https://doi.org/10.5880/fidgeo.2023.031.

Declaration of Competing Interest

The authors declare that they have no known competing financial interests or personal relationships that could have appeared to influence the work reported in this paper.

Acknowledgement

We would like to extend our sincere gratitude to Lioba Virchow (GFZ Potsdam), Antje Musiol, Rami Al Abed and Christina Günter (Universität Potsdam) for their invaluable help with sample preparation and analytical measurements. We also warmly thank Pierre Bouvier (Néel Institute, CNRS) for helping in setting up the Raman measurements in the autoclave, and for his critical look over the acquisition procedures. The quality of our contribution greatly improved by the constructive comments and suggestions of Dionysis Foustoukos, Xiaolin Wang, an anonymous reviewer and the editor Jeff Catalano. This study was made possible through the research initiative funding of Universität Potsdam.

References

Alberty, R., 1969. Standard Gibbs free energy, enthalpy, and entropy changes as a function of pH and pMg for several reactions involving adenosine phosphates. Biological Chemistry 244, 3290-3302.

Asano, T., Noble, W. J., 1978. Activation and reaction volumes in solution. Chemical Reviews 78, 407-489.

Bains, W., Xiao, Y., Yu, C., 2015. Prediction of the Maximum Temperature for Life Based on the Stability of Metabolites to Decomposition in Water. Life 5, 1054-1100.

Bar-On, Y. M., Phillips, R., Milo, R., 2018. The biomass distribution on Earth. Proceedings of the National Academy of Science 115, 6506-6511.

Bassett, W., Shen, A., Bocknum, M., Chou, I.-M., 1993. Hydrothermal studies in a new diamond anvil cell up to 10 GPa and from -190 °C to 1200 °C. Pure and applied geophysics 141, 487-495.

Beulig, F., Schubert, F., Adhikari, R. R., Glombitza, C., Heuer, V. B., Hinrichs, K.-U., Homola, K. L., Inagaki F., Jørgensen, B. B., Kallmeyer, J., Krause, S. J. E., Morono, Y., Sauvage, J., Spivack, A. J., Treude T., 2022. Rapid metabolism fosters microbial survival in the deep, hot subseafloor biosphere. Nature Communications 13, 312.

Blöchl, E., Rachel, R., Burggraf, S., Hafenbradl, D., Jannasch, H., Stetter, K., 1997. Pyrolobus fumarii, gen. and sp. nov., represents a novel group of archaea, extending the upper temperature limit for life to 113 °C. Extremophiles 1, 14-21.

Bridgman, P., 1914. The coagulation of Albumen by pressure. Journal of Biological Chemistry 19, 511-512.

Bruyère, R., Prat, A., Goujon, C., Hazemann, J.-L., 2008. A new pressure regulation device using high pressure isolation valves. Journal of Physics: Conference Series 121, 122003.

Buisson, D., Sigel, H., 1974. Significance of binary and ternary copper (II) complexes for the promotion and protection of adenosine 5′-di- and triphosphate toward hydrolysis. Biochimica et Biophysica Acta - General Subjects 343, 45-63.

Burgot, J.-L., 2020. Thermodynamics in Bioenergetics, first ed. CRC Press, Boca Raton (Fl.).

Cannon, W. B., 1929. Organization for physiological homeostasis. Physiological reviews 9, 399-431.

Corliss, J. B., Ballard, R. D., 1977. Oases of Life in the Cold Abyss. National Geographic 152, 440-453.

Covington, A., Paabo, M., Robinson, R., Bates, R., 1968. Use of the glass electrode in deuterium oxide and the relation between the standardized pD (paD) scale and the operational pH in heavy water. American Chemical Society 40, 700-706.

822 Dalmasso, C., Oger, P., Selva, G., Courtine, D., L'Haridon, S., Garlaschelli, A., Roussel
823 E., Miyazaki J., ReveillaudJ., Jebbar M., Takai K., Maignien L., Alain, K., 2016. Thermococ-
824 cus piezophilus sp. nov., a novel hyperthermophilic and piezophilic archaeon with a broad
825 pressure range for growth, isolated from a deepest hydrothermal vent at the Mid-Cayman
826 Rise. Systematic and Applied Microbiology 39, 440-444.
827
828 Daniel, R. M., van Eckert R., Holden, J. F., Truter, J., Cowan, D. A., 2004. The stability
829 of biomolecules and the implications for life at high temperatures. Geophysical Monograph
830 Series 144, 25-39.
831
832 Delaney, J. R., Robigou, V., McDuff, R. E., Tivey, M. K., 1992. Geology of a vigorous
833 hydrothermal system on the Endeavour segment, Juan de Fuca ridge. Geophysical Research,
834 97, 19663-19682.
835
836 Edwards, K., Wheat, C., Sylvan, J., 2011. Under the sea: microbial life in volcanic oce-
837 anic crust. Nature Reviews Microbiology 9, 703-712.
838
839 Eisenberg, D., Kauzmann, W., 1969. The structure and properties of water. Oxford Uni-
840 versity Press, London.
841
842 Eysel, H. H., Lim, K. T., 1988. Raman intensities of phosphate and diphosphate ions in
843 aqueous solution. Journal of Raman Spectroscopy 19, 535-539.
844
845 Fukui, K., Kato, K., Kodama, T., Ohta, H., Shimamoto, T., Shimono, T., 1988. Kinetic
846 study of a change in intracellular ATP level associated with aerobic catabolism of ethanol
847 Streptococcus mutans. Journal of Bacteriology 170, 4589-4593.
848
849 Gadkari, D., Stolp, H., 1976. Energy metabolism of Bdellovibrio bacteriovorus. II. P/O
850 ratio and ATP pool turnover rate. Arch Microbiology 108, 125-132.
851
852 Gajewski, E., Steckler, D., Goldberg, R., 1986. Thermodynamics of the Hydrolysis of
853 Adenosine 5'-triphosphate to Adenosine 5'-diphosphate. Biological Chemistry 261, 12733-
854 12737.
855
856 Glickson, D., Kelley, D., Delaney, J., 2007. Geology and hydrothermal evolution of the
857 Mothra Hydrothermal Field, Endeavour Segment, Juan de Fuca Ridge. Geochemistry, Geo-
858 physics, Geosystems 8, 6.
859
860 Golyshina, O. V., Golyshin, P. N., Timmis, L. N., Ferrer, M., 2006. The 'pH optimum
861 anomaly' of intercellular enzymes of Ferroplasma acidiphilum. Environmental Microbiology
862 8, 416-425.
863
864 Guildner, L. A., Johnson, D.P., Jones, F. E., 1976. Vapor pressure of water at its triple
865 point. Journal of Research of the National Bureau of Standards 80A, 505-521.
866
867 Helgeson, H., Kirkham, D., Flowers, G. 1981. Theoretical prediction of the thermody-
868 namic behavior of aqueous electrolytes by high pressures and temperatures; IV, Calculation
869 of activity coefficients, osmotic coefficients, and apparent molal and standard and relative
870 partial molal properties to 600. American Journal of Science 281, 1249-1516.
871

Heuer, V. B., Inagaki, F., Morono, Y., Kubo, Y., Spivack, A. J., Viehweger, B., Treude, T., Beulig, F., Schubotz, F., Tonai, S., Bowden, S. A., Cramm, M., Henkel, S., Hirose, T., Homola, K., Hoshino, T., Akira, I., Imachi, H., Kamiya, N., Kaneko, M., Lagostina, L., Manners, H., MacCleland, H.-L., Metcalfe, K., Okutsu N., Pan, D., Raudsepp, M. J., Sauvage, J., Tsang, M.-Y., Wang, D. T., Whitaker, E., Yamamoto, Y., Yang, K., Maeda, L., Adhikari, R. R., Glombitza, C., Hamada, Y., Kallmeyer, J., Wendt, J., Wörmer, L., Yamada, Y., Kinoshita, M., Hinrichs, K. U., 2020. Temperature limits to deep subseafloor life in the Nankai Trough subduction zone. Science 370, 1230-1234.

Heyde, M. E., Rimai, L., 1971. A Raman spectroscopic study of the interaction of Ca^{2+} and Mg^{2+} with the triphosphate moiety of adenosine triphosphate in aqueous solution. Biochemistry 10, 1121-1128.

Hulett, H., 1970. Non-enzymatic Hydrolysis of Adenosine Phosphates. Nature 228, 1248-1249.

IAPWS, The International Association for the Properties of Water and Steam, 2011. Revised Release on the Pressure along the Melting and Sublimation Curves of Ordinary Water Substance, http://www.iapws.org/relguide/MeltSub2011.pdf, (accessed 03rd May 2024).

Jebbar, P. M., Oger, M., 2010. The many ways of coping with pressure. Research Microbiology 161, 799-809.

Jorgensen, B. B., 2011. Deep subseafloor microbial cells on physiological standby. Proceedings of the National Academy of Science 108, 18193-18194.

Journaux, B., Brown, J. M., Pakhomova,A., Collings, I. E., Petitgirard, S., Espinoza, P., Ballaran, T. B., Vance, S. D., Ott, J., Cova, F., Garbarino, G., Hanfland, M., 2020. Holistic approach for studying planetary hydrospheres: Gibbs, elasticity and the water phase diagram to 2300 MPa. Journal of Geophysical Research: Planets 125, 1.

Kamb, B., Davis, B. L., 1964. Ice VII, The densest form of ice. Proceedings of the National Academy of Science 6, 1433-1439.

Kaplan, J. H., Forbush III, B., Hoffman, J. F., 1978. Rapid Photolytic Release of Adenosine S'-Triphosphate from a Protected Analogue: Utilization by the Na:K Pump of Human Red Blood Cell Ghosts. American Chemical Society 17, 1929-1935.

Kaplan, J. H, Somlyo A. P., 1989. Flash photolysis of caged compounds: New tools for cellular physiology. Trends in Neuroscience 12, 54-59.

Kauzmann, W., 1987. Thermodynamics of unfolding. Nature 325, 763-764.

Kelm, H., Palmer, D.A., 1978. Determination and Interpretation of Volumes of Activation. In: Kelm, H. (eds) High Pressure Chemistry. NATO Advanced Study Institutes Series, vol 41. Springer, Dordrecht.

Kengen, S. W., Tuininga, J. E., de Bok, F. A., Stams, A. J., de Vos, W. M., 1995. Purification and Characterization of a Novel ADP-dependent Glucokinase from the Hyperthermophilic Archaeon Pyrococcus furiosus. Biological Chemistry 270, 30453-30457.

Kestin, J., Sengers, J., Kamgar-Parsi, B., Levelt Sengers, J. M. H., 1984. Thermophysical Properties of Fluid H_2O. J. Physical and Chemical Reference Data 13, 175-183.

Khan, M. M. T., Mohan, M. S., 1974. Kinetics of adenosine-5'-triphosphate hydrolysis. Journal of Inorganic and Nuclear Chemistry 36, 707-709.

LaRowe, D., Helgeson, H., 2006. Biomolecules in hydrothermal systems: Calculation of the standard molal thermodynamic properties of nucleic-acid bases, nucleosides, and nucleotides at elevated temperatures and pressures. Geochimica et Cosmochimica Acta 70, 4680–4724.

Leibrock, E., Bayer, P., Lüdemann, H., 1995. Nonenzymatic hydrolysis of adenosinetriphosphate (ATP) at high temperatures and high pressures. Biophysical Chemistry 54, 175-180.

Legrain, C., Demarez M., Glansdorff, N., Piêrard, A., 1995. Ammonia-dependent synthesis and metabolic channelling of carbamoyl phosphate in the hyperthermophilic archaeon Pyrococcus furiosus. Microbiology 141, 1093-1099.

Lipmann, F., 1941. Metabolic generation and utilization of phosphate bond energy. In Lipmann (Ed.), Advances in Enzymology and Related Subjects. Interscience Publishers, New York, pp. 99-162.

Louvel, M., Bordage, A., Silva-Cadoux, C. D., Testemale, D., Lahera, E., Net, W., Geaymond, O., Dubessy J., Argoud R., Hazemann, J.-L., 2015. A HP/HT setup for in situ Raman spectroscopy of supercritical fluids. Molecular Liquids 205, 54-60.

Marshall, W. L., Begun, G.M., 1989. Raman spectroscopy of aqueous phosphate solutions at temperatures up to 450 °C, Journal of Chemical Society, Faraday Transactions 2: Molecular and Chemical Physics 85, 1963-1978.

Marshall, W. L., Franck, E. U., 1981. Ion product of water substance, 0-1000 °C, 1-10 000 bars new international formulation and its background. Journal of Physical and Chemical Reference Data 10, 295-304.

Mathlouthi, M., Seuvre, A.-M., Koenig, J. L., 1984. F.T.-I.R. and laser-Raman spectra of adenine and adenosine. Carbohydrate Research 131, 1-15

Mayer, G., Heckel A., 2006. Biologically Active Molecules with a "Light Switch". Angewandte Chemie 45, 4900-4921.

Merino, N., Aronson, H. S., Bojanova, D. P., Feyhl-Buska, J., Woong, M. L., Zhang, S., Giovannelli, D., 2019. Living at the Extremes: Extremophiles and the Limits of Life in a Planetary Context. Frontiers in Microbiology 10, 780.

Moeller, C., Schmidt, C., Guyot, F., Wilke, M., 2022. Hydrolysis rate constants of ATP determined in situ at elevated temperatures. Biophysical Chemistry 290, 106878.

[dataset] Moeller, C., Schmidt, C., Testemale, D., Guyot, F., Kohk, M., Wilke, M., 2024. Database of in-situ Raman spectra from Na_2H_2ATP solutions at 80,100 and 120 °C and up to

1666 MPa for determination of the rate constant of the ATP hydrolysis. GFZ Data Services v1. doi.org/10.5880/fidgeo.2023.031.

Mohana-Borges, R., Silva, J. L., Ruiz-Sanz J., de Prat-Gay, G., 1999. Folding of a pressure-denatured model protein. Proceedings of the National Academy of Science 96, 7888-7893.

Peng, D.-Y., Robinson, D., 1976. A New Two-Constant Equation of State. American Chemical Society 15, 59-64.

Petrenko, V. F., Whitworth, R.W., 1999. Physics of ice. Oxford University Press, Oxford.

Phillips, R., George, S., Rutman, R., 1966. Thermodynamic Studies of the Formation and Ionization of the Magnesium (II) Complexes of ADP and ATP over the pH Range 5 to 9. American Chemical Society 88, 2631-2640.

Plümper, O., King, H., Geisleier, T., Liu, Y., Pabst, S., Savov, I., Rost, D., Zack, T., 2017. Subduction zone forearc serpentinites as incubators for deep microbial life. Proceedings of the National Academy of Science 114, 4324-4329.

Preston, C. M., Adams, W. A., 1979. A laser Raman spectroscopy study of aqueous orthophosphate salts, Journal of Physical Chemistry 83, 814-821.

Ramirez, F., Marecek, J. F., Szamosi, J., 1980. Magnesium and calcium ion effects on hydrolysis rates of adenosine 5'-triphosphate. Journal of Organic Chemistry 45, 4748–4752.

Robie, R., Hemingway, B., 1978. Thermodynamic properties of minerals and related substances at 298.15 K and 1 bar (105 pascals) pressure and at higher temperatures. U. S. Geological Survey Bulletin 1452.

Rudolph, W. W., 2010. Raman- infrared -spectroscopic investigations of dilute aqueous phosphoric acid solutions. Dalton Transactions 39, 9642-9653.

Schmidt, C., 2009. Raman spectroscopic study of a H_2O + Na_2SO_4 solution at 21-600°C and 0.1 MPa to 1.1 GPa: Relative differential v_1-SO_4^{2-} Raman scattering cross sections and evidence of the liquid-liquid transition. Geochimica et Cosmochimica Acta 73, 425-437.

Schmidt, C., 2014. Raman spectroscopic determination of carbon speciation and quartz solubility in H_2O+Na_2CO_3 fluids to 600 °C and 1.53 GPa. Geochimica et Cosmochimica Acta 145, 281-296.

Schmidt, C., Chou, I.-M., 2012. The Hydrothermal Diamond Anvil Cell (HDAC) for Raman spectroscopic studies of geological fluids at high pressures and temperatures. - In: Dubessy, J., Caumon, M.-C., Rull, F., (Eds.), Raman spectroscopy applied to Earth sciences and cultural heritage (EMU Notes in Mineralogy), Mineralogical Society of Great Britain and Ireland, pp. 247-276.

Schmidt, C., Ziemann, M., 2000. In-situ Raman spectroscopy of quartz: A pressure sensor for hydrothermal diamond-anvil cell experiments at elevated temperatures. American Mineralogist 85, 1725-1734.

Sharma, A., Scott, J., Cody, G., Fogel, M., 2002. Microbial Activity at Gigapascal Pressures. Science 295, 1514-1516.

Shock, E., Helgeson, H., 1988. Calculation of the thermodynamic and transport properties of aqueous species at high pressures and temperatures: Correlation algorithms for ionic species and equation of state predictions to 5 kb and 1000 °C. Geochimica et Cosmochimica Acta 52, 2009-2036.

Shock, E., Helgeson, H., Sverjensky, D., 1989. Calculation of the thermodynamic and transport properties of aqueousspeciesat high pressures and temperatures: Standard partial molal properties of inorganic neutral species. Geochimica et Cosmochimica Acta 53, 2157-2183.

Shock, E., Sassani, D., Willis, M., Sverjensky, D., 1997. Inorganic species in geologic fluids: Correlations among standard molal thermodynamic properties of aqueous ions and hydroxide complexes. Geochimica et Cosmochimica Acta 61, 907-950.

Shvarov, Y., 1999. Algorithmization of the Numeric Equilibrium Modeling of Dynamic Geochemical Processes. Geochemistry International 37, 571-576.

Sinha, N., Nepal, S., Kral, T., Kumar, P., 2017. Survivability and growth kinetics of methanogenic archaea at various pHs and pressures: implications for deep subsurface life on Mars. Planetary Space Science 136, 15-24.

Sridharan, S., Kurzawa, M., Werner, T., Günthner, I., Helm, D., Huber, W., Bantscheff, M., Savitski, M. M., 2019. Proteome-wide solubility and thermal stability profiling reveals distinct regulatory roles for ATP. Nature Communication 10, 1-13.

Suzuki, S., Higashiyama, T., Nakahara, A. 1978. Nonenzymatic hydrolysis reactions of adenosine 5′-triphosphate and its related compounds-III: Catalytic aspects of some cobalt (III) complexes in ATP-hydrolysis. Bioinorganic Chemistry 8, 277-289.

Sverjensky, D. A., Harrison, B., Azzolini, D., 2014. Water in the deep Earth: The dielectric constant and the solubilities of quartz and corundum to 60 kb and 1200 °C. Geochimica et Cosmochimica Acta 129, 125-145.

Takai, K., Nakamura, K., Toki, T., Horikoshi, K., 2008. Cell proliferation at 122°C and isotopically heavy CH_4 production by a hyperthermophilic methanogen under high-pressure cultivation. Proceedings of the National Academy of Science 105, 10949-10954.

Testemale, D., Argoud, R., Geaymound, O., Hazemann, J.-L., 2005. High pressure/high temperature cell for x-ray absorption and scattering techniques. Review of Scientific Instruments 76, 043905.

Tetas, M., Lowenstein, J. M., 1963. The Effect of Bivalent Metal Ions on the Hydrolysis of Adenosine Di- and Triphosphate. Biochemistry 2, 350-357.

Urayama, P., Phillips, G., Gruner, S., 2002. Probing Substates in Sperm Whale Myoglobin Using High-Pressure Crystallography. Structure 10, 51-60.

1072 Walrafen, G. E., Abebe, M., Mauer, F. A., Block S., Piermarini, G. J., Munro, R., 1982.
1073 Raman and x-ray investigations of ice VII to 36.0 GPa. Journal of Chemical Physics 77,
1074 2166-2174.
1075
1076 Westheimer, F., 1961. The magnitude of the primary kinetic isotope effect for compounds
1077 of hydrogen and deuterium. Chemical reviews 61, 265-273.
1078
1079 Yayanos, A. A., 2002. Are Cells Viable at Gigapascal Pressures? Science 297, 295.
1080
1081 Zilversmit, D., 1955. Meaning of Turnover in Biochemistry. Nature 175, 863.